

**PREPARATION AND EVALUATION OF MAGNETIC
NANOCOMPOSITE FILMS AND FIBERS CONTAINING α'' -Fe₁₆N₂
NANOPARTICLES**

(窒化鉄ナノ粒子を複合した磁性体ナノコンポジットフィルムおよびファイバ
ーの合成と性能評価)

By

CHRISTINA WAHYU KARTIKOWATI

HIROSHIMA UNIVERSITY

SEPTEMBER 2017

**PREPARATION AND EVALUATION OF MAGNETIC
NANOCOMPOSITE FILMS AND FIBERS CONTAINING α'' -Fe₁₆N₂
NANOPARTICLES**

(窒化鉄ナノ粒子を複合した磁性体ナノコンポジットフィルムおよびファイバ
ーの合成と性能評価)

A Thesis submitted to
The Department of Chemical Engineering
Graduate School of Engineering
Hiroshima University

By

CHRISTINA WAHYU KARTIKOWATI

In Partial Fulfillment of the Requirements
For the Degree of
Doctor of Engineering

Hiroshima University
SEPTEMBER 2017

Approved by
Associate Professor Takashi Ogi
Advisor

Abstract

Magnetic materials play a key role in modern life as they facilitate the conversion of electrical to mechanical energy, transmission and distribution of electric power, microwave communications, and data storage systems. Nowadays, magnetic materials are used in various advanced devices, such as motor, recorder data devices, biomedical, sensor, spintronic devices, ferrofluid-related devices, etc. Until now, permanent magnet has been continuously developed in response to the growing demand for higher volume-specific magnetic power to support the advancement of motors, generators, and other energy-related applications. These broad applications require a magnetic material with high energy product. Having the highest magnetic moment and high uniaxial magnetic anisotropy among any ferromagnetic material, α'' -Fe₁₆N₂ nanoparticles (NPs) emerge as a potential rare-earth-free permanent magnet. However, these NPs have a high magnetic interaction among the NPs and a small magnetic coercivity. These problems can be solved by structuration of α'' -Fe₁₆N₂ NPs. α'' -Fe₁₆N₂ NPs were synthesized by nitridation and then followed by dispersion to break-up the agglomerates NPs, can be structurized in a nanocomposite form such as film and fiber. Magnetic field was applied during nanostructuration to align the magnetic moment of α'' -Fe₁₆N₂ NPs. A magnetic field was applied during nanostructuration to align the magnetic moment of α'' -Fe₁₆N₂ NPs for enhancing the magnetic properties. Therefore, detailed understanding on the preparation of α'' -Fe₁₆N₂ nanocomposites under applied magnetic field and their magnetic performance are highly desired.

In this dissertation, preparation and evaluation of α'' -Fe₁₆N₂ nanocomposite films via spin coating and fibers via electrospinning are systematically investigated. An external magnetic field was applied during the nanocomposites preparation to align the magnetic moment of the α'' -Fe₁₆N₂ NPs. The effect of this applied magnetic field on the nanocomposite morphology, structure and magnetic properties was studied. The major contents of this dissertation are listed as follow.

Chapter 1 describes the background and the motivation of this research. Basic theoretical explanation and review of previous researches on the α'' -Fe₁₆N₂ magnetic materials as well as an overview of the magnetic nanocomposite materials are also provided.

Chapter 2 explains the synthesis of α'' -Fe₁₆N₂ nanocomposite films via spin-coating under 0.1T of applied magnetic field as well as effects of these magnetic field on the magnetic performance. A ~ 1 μm densely packed assemblies of the NPs were formed and aligned

perpendicularly in a film. The application of the magnetic field during film formation increased the magnetic coercivity (Hc) and remanence (Mr) values of the resulted films by 23% and 55%, respectively.

In Chapter 3, an effect of applied magnetic field strength on the magnetic performance of α'' -Fe₁₆N₂ nanocomposite films via spin-coating are discussed. The film with thickness of 1 μ m was prepared with same method as in the chapter 2. However, some external magnetic fields of strength 0, 0.6, 0.9, or 1.2 T were applied to examine the magnetic orientations of α'' -Fe₁₆N₂/Al₂O₃ NPs films. X-ray diffraction and SQUID analyses showed the relationship between the aligned orientation of the NPs and their magnetic properties; magnetic coercivity, remanence, and maximum energy product enhanced by 24%, 66%, and 160%, respectively, with increase in magnetic orientation of 35%. The shape of hysteresis loops of the films approached to rectangular by increasing the vertically applied magnetic field. These results were further verified by applying the magnetic field horizontally.

The effect of applied magnetic field on diameter of α'' -Fe₁₆N₂/PVP nanocomposite fiber via electrospinning and its magnetic performance are investigated in Chapter 4. An external magnetic field of 0.1 T was applied during process of electrospinning. α -Fe NPs which is soft magnet was also used to investigate the effect of NP magnetic strength on the nanocomposite fiber properties such as, diameter and magnetic properties. These NPs were dispersed in toluene using low-energy beads-mill dispersion to prepare magnetic NPs slurry. The magnetic NPs slurry was mixed with a 15 wt % of PVP solution to make a ferrofluid precursor for electrospinning with two different loadings of 16.5wt% and 28.4 wt% of magnetic NPs. The PVP solution was obtained by dissolving 15 wt% PVP in a mixture of toluene and methanol with a mass ratio of 1:1. SEM and TEM analysis results showed that the applying the magnetic field in the same direction as the electric field resulted in smaller and more uniform fiber diameters. Further, nanocomposite fibers containing α'' -Fe₁₆N₂ had smaller diameters than those containing α -Fe NPs. In addition, magnetic hysteresis curves showed an enhancement of the magnetic coercivity and remanence by 23% and 22%, respectively.

Chapter 5 contains the summary of all chapters and direction for further investigation.

Contents

Abstract	i
Content	iii
List of Figures	v
List of Tables	viii
1. Introduction	1
1.1 Importance of magnetic materials in human life	1
1.2 Magnetic properties of ferromagnetic materials	1
1.3 α'' -Fe ₁₆ N ₂ magnetic material	3
1.3.1 Synthesis of single-domain α'' -Fe ₁₆ N ₂ nanoparticles	5
1.3.2 Dispersion of α'' -Fe ₁₆ N ₂ nanoparticles	6
1.4 Nanostructured magnetic materials	8
1.4.1 Magnetic nanocomposite film	10
1.4.2 Magnetic nanocomposite fiber	10
1.5 Objectives and outline of the dissertation	12
1.6 References	14
2. Synthesis of well-dispersed single-domain α''-Fe₁₆N₂ nanocomposite films under magnetic field	19
2.1 Introduction	19
2.2 Experimental	20
2.2.1 Preparation of raw materials	20
2.2.2 Preparation of magnetic film	20
2.2.3 Characterization	21
2.3 Results and discussion	22
2.3.1 Physicochemical properties of core–shell α'' -Fe ₁₆ N ₂ /Al ₂ O ₃ NPs	22
2.3.2 Structure of magnetically oriented film	23
2.3.3 Magnetic properties of magnetically oriented film	26
2.4 Conclusion	28
2.5 References	28

3. Effect of magnetic field strength on alignment of single domain α''-Fe₁₆N₂ nanocomposite film	31
3.1 Introduction	31
3.2 Experimental	32
3.2.1 Preparation of raw materials	32
3.2.2 Preparation of magnetically aligned films	32
3.2.3 Characterization	34
3.3 Results and discussion	34
3.4 Conclusion	42
3.5 References	42
4. Synthesis of α''-Fe₁₆N₂/Polyvinylpyrrolidone magnetic nanocomposite fibers under magnetic field	46
4.1 Introduction	46
4.2 Experimental	47
4.2.1 Preparation of raw materials	47
4.2.2 Preparation of ferrofluid for electrospinning	48
4.2.3 Magneto-electrospinning	48
4.2.4 Characterization	49
4.3 Results and discussion	49
4.3.1 Core-shell α'' -Fe ₁₆ N ₂ /Al ₂ O ₃ and α -Fe/Al ₂ O ₃ NPs	49
4.3.2 Electrospun PVP fibers	50
4.3.3 Electrospun magnetic nanocomposite fibers	51
4.3.4 Evaluation of electrospun magnetic nanocomposite fibers	53
4.3.4.1 Effect of flow rate on the fiber diameter	55
4.3.4.2 Effect of applied magnetic field on fibers diameter	57
4.3.5 Magnetic properties of electrospun magnetic nanocomposite fibers	57
4.4 Conclusion	59
4.5 References	60
5. Summary and conclusion	63

List of Figures

Figure 1.1	Applications of magnetic materials.	1
Figure 1.2	Magnetic hysteresis loop.	3
Figure 1.3	Fe-N phase diagram based on the nitridation process at atmospheric pressure.	4
Figure 1.4	Crystal structure of α'' -Fe ₁₆ N ₂ phase.	5
Figure 1.5	The schematic diagram of synthesis of α'' -Fe ₁₆ N ₂ /Al ₂ O ₃ magnetic nanoparticles.	6
Figure 1.6	SEM image (a), X-ray diffraction (b), and magnetic hysteresis loop (c) of α'' -Fe ₁₆ N ₂ /Al ₂ O ₃ MNPs prepared by nitridation.	6
Figure 1.7	Schematic diagram of all separator beads mill machine.	7
Figure 1.8	Hysteresis curves of α'' -Fe ₁₆ N ₂ /Al ₂ O ₃ before and after dispersion process. (b) Schematic illustration of magnetic interaction among single domain of α'' -Fe ₁₆ N ₂ /Al ₂ O ₃ NPs under applied magnetic field. The red arrow in the circles indicates magnetic dipole moment.	8
Figure 1.9	Illustration of nanostructuring of α'' -Fe ₁₆ N ₂ nanoparticles.	9
Figure 1.10	Organization and structure of chapters in the present dissertation.	13
Figure 2.1	Schematic illustration of the preparation process of magnetically oriented films from core-shell α -Fe/Al ₂ O ₃ NPs.	21
Figure 2.2	Physicochemical properties of as-prepared and dispersed core-shell α'' -Fe ₁₆ N ₂ /Al ₂ O ₃ NPs. (a) SEM image and (b) EELS analysis of as-prepared NPs. (c) TEM image of dispersed NPs. (d) XRD pattern of as-prepared and dispersed NPs. The insets in (a) show cross sectional TEM images of the particle. The red line in the top-right inset of (a) is the scanned range for the EELS line analysis.	23
Figure 2.3	SEM images of cross section of the core-shell α'' -Fe ₁₆ N ₂ /Al ₂ O ₃ NPs spin-coated film viewed at a tilt angle of 40°: (a) without resin and no applied magnetic field and (b) with resin under applied magnetic field. Inset in (b) shows the cross section of the oriented film. Dashed lines show the average film thickness.	24
Figure 2.4	Illustration of magnetic particle direction in several conditions: no applied magnetic field, under magnetic field and after fixation using adhesive resin.	25
Figure 2.5	XRD patterns of vertically and randomly oriented of the α'' -Fe ₁₆ N ₂ /Al ₂ O ₃ magnetic NPs films.	26
Figure 2.6	Magneto-optic Kerr effect analysis of the core-shell α'' -Fe ₁₆ N ₂ /Al ₂ O ₃ NPs films. The red and black curves show the hysteresis of the films prepared under the presence and absence of an applied magnetic field, respectively.	27

Figure 2.7	Hysteresis loops of the core-shell α'' -Fe ₁₆ N ₂ /Al ₂ O ₃ NPs films measured on a SQUID magnetometer at 300 K for randomly and vertically oriented films.	28
Figure 3.1	Schematic diagram of preparation of magnetically aligned α'' -Fe ₁₆ N ₂ /Al ₂ O ₃ NPs film.	33
Figure 3.2	SEM (a) and TEM (b) images of α'' -Fe ₁₆ N ₂ /Al ₂ O ₃ NPs; inset shows cross-sectional TEM image.	34
Figure 3.3	SEM images of surface and cross-section of spin-coated α'' -Fe ₁₆ N ₂ /Al ₂ O ₃ NP film under vertical magnetic field, viewed at a tilt angle of 40°: low (a) and high (b) magnification.	35
Figure 3.4	XRD patterns of α'' -Fe ₁₆ N ₂ /Al ₂ O ₃ NPs and films under various applied magnetic fields.	36
Figure 3.5	Hysteresis loops of α'' -Fe ₁₆ N ₂ /Al ₂ O ₃ NPs and films under various applied magnetic fields; inset shows changes in coercivity (H _c).	38
Figure 3.6	Maximum energy product and magnetic coercivity of the α'' -Fe ₁₆ N ₂ /Al ₂ O ₃ NP film as a function of the applied magnetic field.	40
Figure 3.7	XRD pattern (a) and magnetic hysteresis loop (b) of α'' -Fe ₁₆ N ₂ /Al ₂ O ₃ NP film under a horizontally applied magnetic field.	41
Figure 3.8	Relationship of magnetic NP alignment with magnetic properties of α'' -Fe ₁₆ N ₂ NP film.	42
Figure 4.1	Schematic diagram of the magneto-electrospinning apparatus.	49
Figure 4.2	SEM and TEM images, and size distributions of core-shell α'' -Fe ₁₆ N ₂ /Al ₂ O ₃ (a), (b), (c) and α -Fe/Al ₂ O ₃ (d), (e), (f) NPs, respectively.	50
Figure 4.3	SEM images and size distributions of electrospun PVP fibers prepared without (a) and with (b) magnetic field.	50
Figure 4.4	XRD patterns of the nanocomposite magnetic fibers with MNP loadings of 28.4 wt%. (a) and (b) are α'' -Fe ₁₆ N ₂ /PVP and α -Fe/PVP magnetic nanocomposite fibers, respectively.	51
Figure 4.5	TEM images of magnetic α'' -Fe ₁₆ N ₂ /PVP nanocomposite fibers produced with an NP loading of 28.4 wt% without (a) and with (b) magnetic field. (c) and (d) are the SAED pattern and HRTEM image of α'' -Fe ₁₆ N ₂ NP inside the fiber. White lines in panels (a) and (b) show the fiber diameter.	52
Figure 4.6	Plots of log d _f (average nanocomposite fiber diameter) against log (Q/I) at different MNP loadings. (a) and (b) are the α'' -Fe ₁₆ N ₂ /PVP and α -Fe/PVP nanocomposite fibers, respectively.	56
Figure 4.7	Hysteresis curves of nanocomposite α'' -Fe ₁₆ N ₂ /PVP magnetic fibers with an MNP loading of 28.4 wt%.	58
Figure 4.8	(a) Initial SQUID analysis of nanocomposite α'' -Fe ₁₆ N ₂ /PVP magnetic fibers with a MNP loading of 28.4 wt%. (b) Schematic diagram of possible	59

magnetic particle directions inside fibers prepared without and with a magnetic field.

List of Tables

Table 1.1	Fundamental magnetic properties of hard magnetic compounds	3
Table 1.2	Methods of the α'' -Fe ₁₆ N ₂ film synthesis	10
Table 3.1	Applied magnetic fields used in preparing various samples	33
Table 3.2	Orientations of vertically aligned α'' -Fe ₁₆ N ₂ NP films	37
Table 3.3	Illustration of alignment phenomena of magnetic orientation in the agglomerated and well-dispersed magnetic NPs	39
Table 4.1	Electrical conductivities of ferrofluid precursors	48
Table 4.2	SEM images of magnetic α'' -Fe ₁₆ N ₂ /PVP and α -Fe/PVP nanocomposite fibers at flow rate of 3 μ l/min	54
Table 4.3	Diameter distributions of nanocomposite fibers prepared without and with applied magnetic field.	55
Table 4.4	Power law exponents of prepared fibers under various conditions	57

Chapter 1

Introduction

1.1 Importance of magnetic materials in modern and future human life

Magnetic materials play a key role in modern and future life as they facilitate the conversion of electrical to mechanical energy, transmission and distribution of electric power, microwave communications, and data storage systems [1]. Nowadays, magnetic materials are widely used in various advanced devices, such as motor [2], recorder data devices [3], biomedical [4, 5], spintronic devices [6] ferrofluid-related devices [7], and advanced technology such as internet of thing (IoT) and artificial intelligence. Advance permanent magnet is one of the most interesting magnetic materials and it is also important for alternative energy technologies [8], such as wind turbine, wave, and tidal power. Until now, permanent magnet has been continuously developed in response to the growing demand for higher volume-specific magnetic energy to support the advancement of motors, generators, and energy applications.

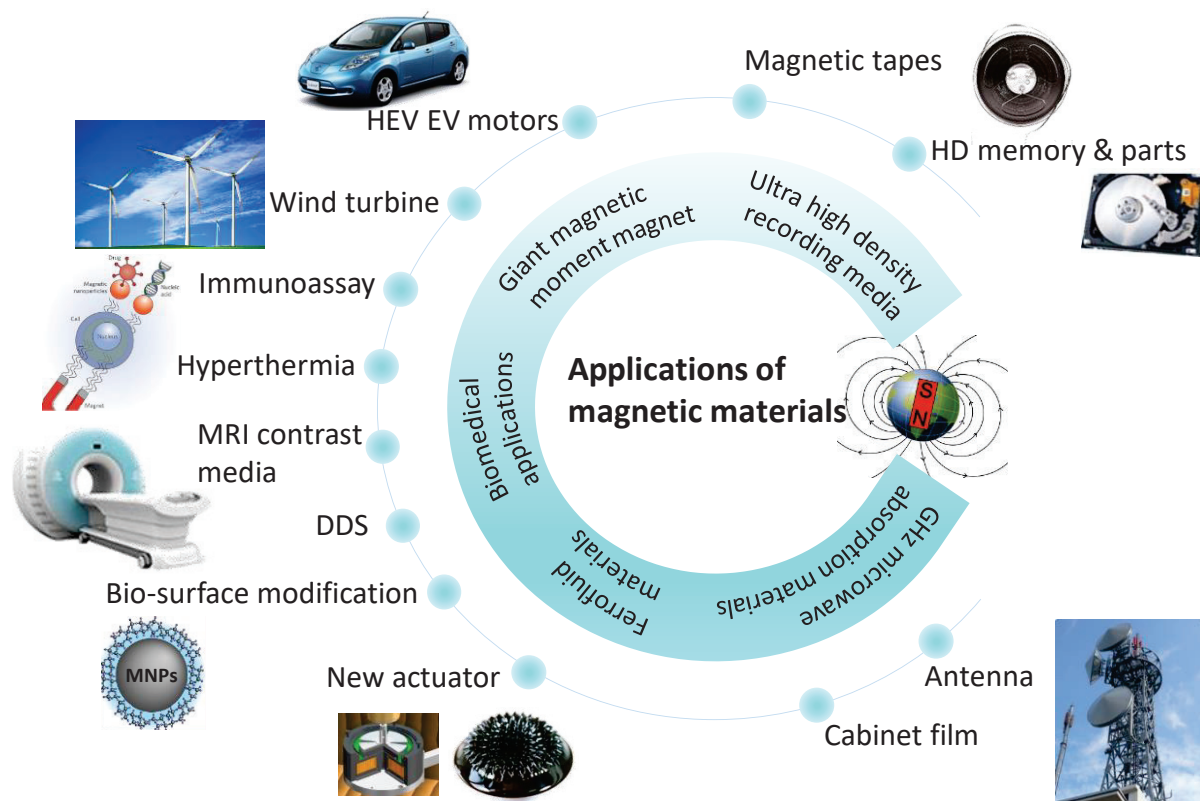


Figure 1.1 Applications of magnetic materials.

1.2 Magnetic properties of ferromagnetic materials

Magnetic material is composed of domains each containing large number of atoms and the magnetic dipoles align one to the other, which exhibits and enhances the collective response even in the absence of a magnetic field. A magnetic particle is composed of single domain if its size decreases below the critical limit (around 100 nm) where this magnetic particle cannot be split up further into domains. Single domain particle has different characteristic from multi-domain particle. Single domain magnetic particle also has higher magnetic performance compared to multi domain particle.

There are four parameters that can describe the strength and the magnetization of the material: coercivity (H_c), saturation magnetization (M_s), remanence (M_r) and energy product ($(BH)_{max}$). H_c is the external field required to reduce the magnetization back to zero, which is related to the minimum energy needed for reversal of the magnetization of the material. M_s shows the maximum value of the magnetization that the material can reach under a sufficient magnetic field, while M_r indicates the residual magnetization at zero applied field. These four parameters can be identified in the hysteresis loop generated in field-dependent magnetization measurement as shown in **Figure 1.2**. There are also two main features that dominate the magnetic properties and give them various special properties: (a) finite-size effects (single-domain or multi-domain structure and quantum confinement of the electrons); (b) surface effects which results from the symmetry breaking of the crystal structure at the surface of the particle, oxidation, dangling bonds, existence of surfactants, surface strain, or even different chemical and physical structures of internal “core” and surface “shell” parts of the nanoparticle.

By evaluating the values of H_c , M_s , M_r and $(BH)_{max}$, magnet material can be classified as soft or hard magnet. Soft magnetic material has low magnetic coercivity and high saturation magnetization of ~ 22 kG, which was used where a high magnetic induction and low losses are needed such as transformer and biomedical applications. Hard magnetic material has H_c higher than 6 kOe and M_s of ~ 16 kG, which was used where a high remanence is required such as permanent magnet and magnetic recording devices.

Driven by many applications of permanent magnets, studies on the synthesis of permanent magnet with higher energy product is growing fast. Basically, in order to achieve high energy product, the material need to have both large magnetization and high magnetic anisotropy. However, up to now, most of the high-energy product of magnet materials contain rare-earth components, such as Nd, Sm, Dy, and Tb. Therefore, the high-energy product of magnet materials without rare-earth components are highly desired for new generation of magnetic materials. α'' - $Fe_{16}N_2$ invented as magnetic material with high saturation magnetization has a good potential as a candidate for new rare-earth-free magnetic material with high magnetic

performance. Several kinds of magnetic materials with their magnetic properties are shown in **Table 1.1**.

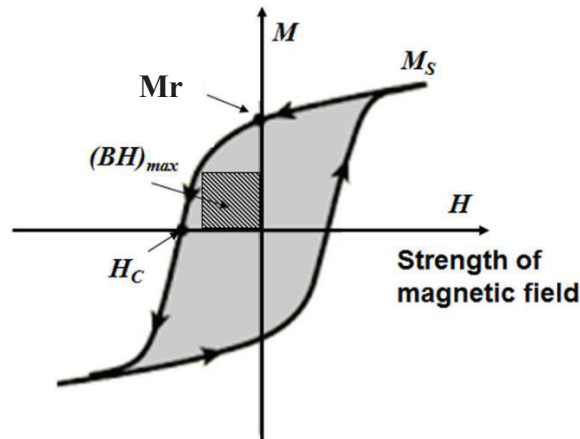


Figure 1.2 Magnetic hysteresis loop.

Table 1.1. Fundamental magnetic properties of hard magnetic compounds

Compound	Saturation magnetization	Anisotropy field	Curie temperature	Theoretical $(BH)_{max}$
$Nd_2Fe_{14}B$	16.0 kG	67 kOe	312 °C	64.0 MGOe
$Sm_2Fe_{17}N_{2.3}$	15.4 kG	140 kOe	476 °C	59.3 MGOe
Sm_2Co_{17}	12.5 kG	65 kOe	920 °C	39.1 MGOe
$SmCo_5$	11 kG	≤ 440 kOe	681 °C	30.2 MGOe
$PrCo_5$	12.3 kG	≥ 145 kOe	620 °C	37.8 MGOe

1.3 α'' - $Fe_{16}N_2$ magnetic material

The interest in iron nitrides arises from their potential applications in high-density magnetic recording media due to their excellent magnetic properties, in catalyst depending on the availability of N-active sites, in biomedical fields since the iron nitrides are relatively less cytotoxic than the iron oxides, and as high wear-resistant and corrosion resistant coating. As compared to other iron compounds, the nitrides possess a greater degree of magnetization than the iron oxides and are more cost-effective than ferromagnetic alloys such as FePt. This iron nitride was found to have attractive magnetic properties due to their high magnetic moment, which is tunable with the concentration of nitrogen in the Fe_xN_y lattice.

Depending on the nitrogen concentration, there is a series of binary Fe-N compounds: γ'' - FeN_y ($y = 0.9-1.0$) with ~ 50 atomic % of N, ζ - Fe_2N with $\sim 33\%$ of N, ϵ - Fe_3N_{1+y} ($y = 0-0.33$) with $\sim 25\%$ of N, γ' - Fe_4N with $\sim 20\%$ of N, and Fe_8N (or α'' - $Fe_{16}N_2$) with $\sim 11\%$ of N [9]. The nitrogen concentration can be synthetically altered to stabilize the Fe-N phases with different

crystal structures, and thus the electronic and magnetic properties can be tuned. The Fe-N phase diagram with magnetic transformation data in the Fe-N system and with the results of nitridation at atmospheric pressure [10, 11] was shown in **Figure 1.3**.

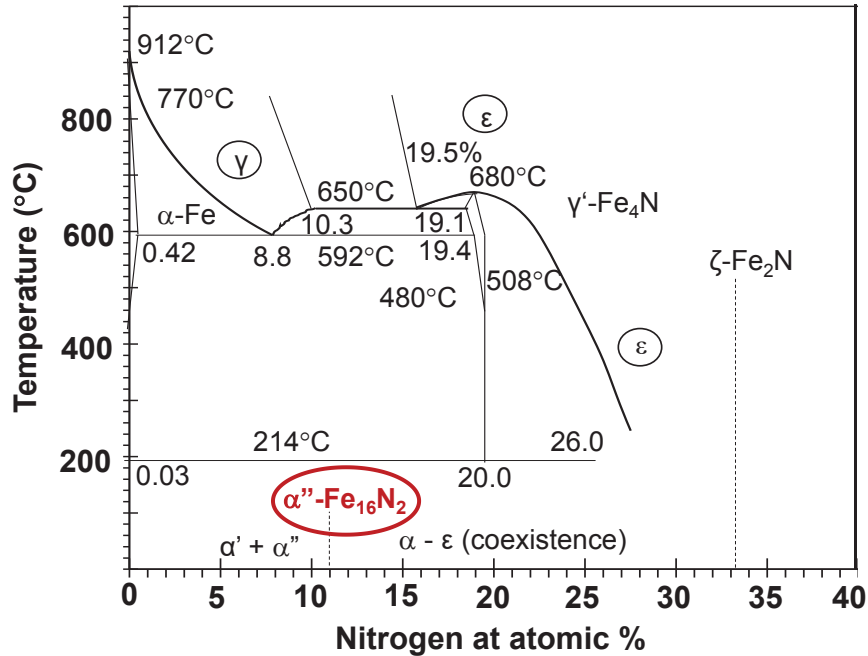


Figure 1.3 Fe-N phase diagram based on the nitridation process at atmospheric pressure.

Among the Fe-N phases, α'' -Fe₁₆N₂ was discovered as Fe-N phase with the highest magnetic moment. α'' -Fe₁₆N₂ has body-centered-tetragonal structure ($a = 5.72 \text{ \AA}$, $c = 6.29 \text{ \AA}$, space group I4/mmm) and is metastable as shown in **Figure 1.4**. One eighth amount of nitrogen occupies the interstitial sites of the α -Fe body-centered cubic lattice on its edge centers in an ordered manner. The unit cell was a $2 \times 2 \times 2$ superlattice of α -Fe, expanded by about 10% along the c -axis by the incorporation of interstitial nitrogen atoms. This electronic structure calculation was resulted in average magnetic moment of 2.4-2.9 μ_B/Fe which is higher than that of BCC Fe (2.2 μ_B). Theoretically, this high magnetic moment is due to the stronger on-site coulomb interaction between the localized 3d electrons in α'' -Fe₁₆N₂. In α'' -Fe₁₆N₂, the nitrogen atoms sit at the center of a cluster of six Fe atoms, and additional Fe atoms stay in between these clusters tend to get localized and contribute to the enhanced magnetic moment.

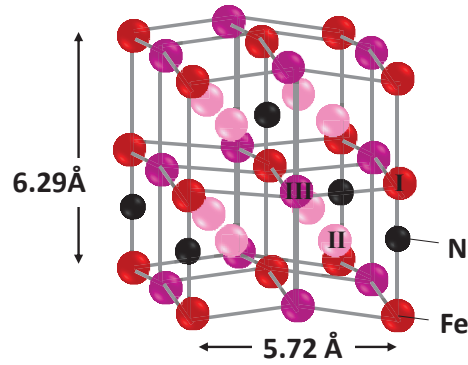
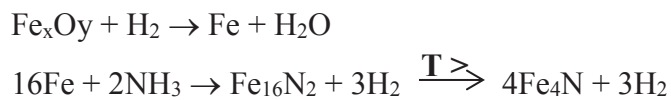


Figure 1.4 Crystal structure of α'' -Fe₁₆N₂ phase.

1. 3. 1 Synthesis of single-domain α'' -Fe₁₆N₂ nanoparticles

Due the fact that single domain magnetic NPs have hinger magnetic performance compared to multi domain NPs, it is preferable to synthesis single domain α'' -Fe₁₆N₂ NPs for further application. α'' -Fe₁₆N₂ phase is formed by nitridation reaction through ammonia (NH₃) gas which was preceded by reduction in hydrogen (H₂) gas flow to form Fe phase. Iron nitride phases are formed by interaction of ammonia with solid Fe at temperatures of $\geq 400^\circ\text{C}$. Iron and the resulting iron nitride phases act as the catalyst in the dissociation of NH₃ to atomic and subsequently to molecular nitrogen and hydrogen. The nitrogen in its atomic state diffuses into the Fe to convert it to its nitride, and the extent of nitridation depends on temperature and time of the reaction and flow rate of NH₃ gas. To get only one Fe-N phase, the nitriding reactions should be optimized at a certain temperature according to Fe-N phase diagram. The formation of iron nitride from Fe NPs is shown in the chemical reaction as follows.



Synthesis of single phase α'' -Fe₁₆N₂ nanoparticles (NPs) have been done for the first time by T. Ogawa et al which have an high Ms value of 234 emu/g and magnetocrystalline anisotropy constant (Ku) of 9.6×10^6 erg/cm³ [12].

T. Ogi et al. and R. Zuhijah et al. have reported the synthesis of single domain core-shell α'' -Fe₁₆N₂/Al₂O₃ magnetic NPs in gas phase process by nitriding plasma synthesized α -Fe/Al₂O₃ magnetic NPs [13-16] as shown in **Figure 1.5**. They successfully synthesized a 50-nm single-domain core-shell α'' -Fe₁₆N₂/Al₂O₃ magnetic NPs with Ms and Hc of 169 emu/g and 3 kOe, respectively as shown in **Figure 1.6**.

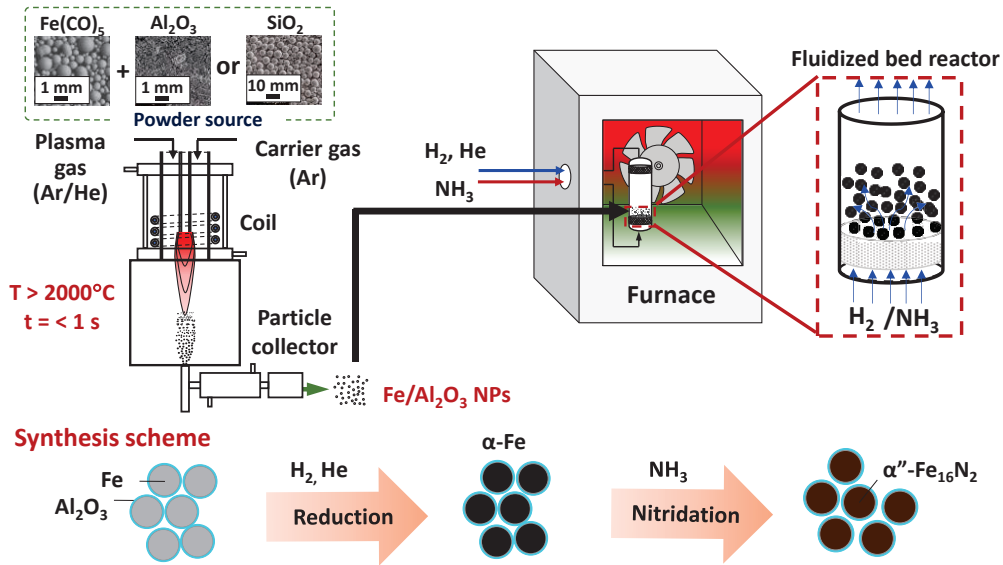


Figure 1.5. The schematic diagram of synthesis of $\alpha''\text{-Fe}_{16}\text{N}_2/\text{Al}_2\text{O}_3$ magnetic nanoparticles.

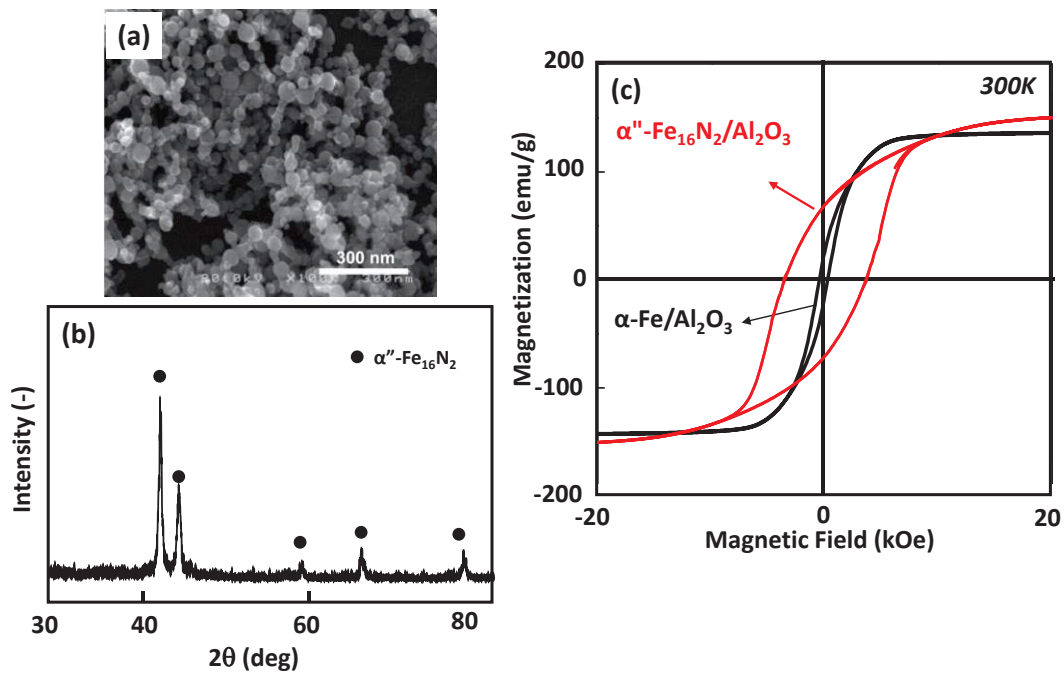


Figure 1.6. SEM image (a), X-ray diffraction (b), and magnetic hysteresis loop (c) of $\alpha''\text{-Fe}_{16}\text{N}_2/\text{Al}_2\text{O}_3$ magnetic nanoparticles prepared by nitridation.

1. 3.2 Dispersion of $\alpha''\text{-Fe}_{16}\text{N}_2$ nanoparticles

Agglomeration and aggregation phenomena still become an unresolved problem in the synthesis of magnetic NPs. As a magnetic NPs, the particle itself easily tend to agglomerate and attach each other due to the lateral magnetic interaction between particles. Moreover, condition during synthesis process also can easily cause the agglomeration and aggregation. In

the case of α'' -Fe₁₆N₂ magnetic NPs synthesized in the gas phase process, high temperature process, particularly in reduction process, will lead to sintering easily. The aggregates and agglomerates particles cannot directly be used for further magnetic nanoparticle alignment. Thus, dispersion after magnetic NP synthesis is highly required and important prior to magnetic nanoparticle alignment.

R. Zuhijah et al. [17, 18] have reported for the first time the dispersion of α'' -Fe₁₆N₂/Al₂O₃ magnetic NPs using low energy beads-mill dispersion as shown in **Figure 1.7**. The dispersibility of these NPs in toluene by a low energy type of all-separator-type beads mill dispersion machine was studied. The core-shell α'' -Fe₁₆N₂/Al₂O₃ NPs were synthesized by simultaneous reduction and nitridation of core-shell plasma-synthesized α -Fe/Al₂O₃ NPs. The effects of the dispersion conditions, i.e., the rotation speed, dispersion time, and bead size, on the dispersion process were thoroughly investigated. The optimum conditions for producing a well-dispersed slurry were examined, and the morphological, physical, and magnetic properties of dispersed core-shell α'' -Fe₁₆N₂/Al₂O₃ NPs were also investigated clearly. Optimum dispersion conditions provide sufficient energy which enabled agglomerated NPs to be broken up into primary particles without destroying their structure. The well-dispersed core-shell α'' -Fe₁₆N₂/Al₂O₃ NPs had the same crystal phase and Ms value as before dispersion. However, the coercivity was significantly changed, because of the rotation of single spin of NPs according to the applied magnetic field and direction as shown in **Figure 1.8**. This magnetization evaluation confirmed that this process is appropriate and essential for the preparation of well-dispersed α'' -Fe₁₆N₂/Al₂O₃ NPs. Thus, the NPs after dispersion will be more applicable for the construction of rare-earth-free high-performance bulk magnet material by restricting the magnetic rotation of the NPs.

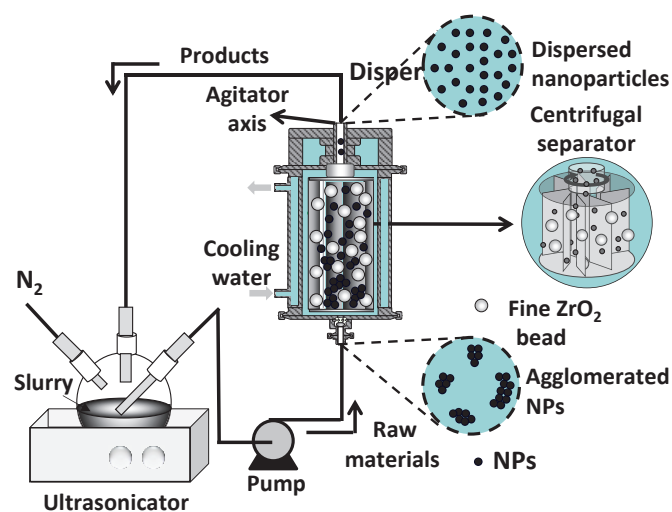


Figure 1.7 Schematic diagram of all separator beads mill machine.

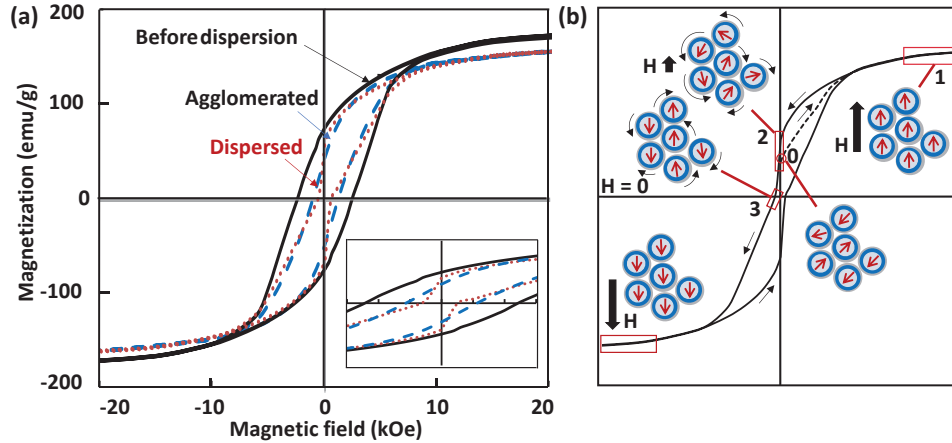


Figure 1.8 Hysteresis curves of α'' -Fe₁₆N₂/Al₂O₃ before and after dispersion process. (b) Schematic illustration of magnetic interaction among single domain of α'' -Fe₁₆N₂/Al₂O₃ NPs under applied magnetic field. The red arrow in the circles indicates magnetic dipole moment.

1.4 Nanostructuring of ferromagnetic materials

As mentioned before, magnetic materials have a broad potential application in modern and future human life. Therefore, the creation of rare-earth-free magnetic materials with high-energy-product is highly desired for their broad application. While it is not possible to find, or create elemental replacement for rare-earth material, the high $(BH)_{\max}$ can be achieved by creating other magnetic systems by control of the crystal structure, the nanostructure and /or the microstructure of alloys and compounds composed of common and plentiful elements. In general, there are two kinds categories of strategy in the development of high energy product rare-earth-free magnetic material: (i) nanocrystal and microstructural development in permanent magnetic nanocomposites with exchanges spring or exchange bias behavior, and ii) crystal structure development to realize high-anisotropy magnetic compounds.

The former describes that this magnet is composed of at least two magnetic phases of complementary magnetic character, e.g., soft magnet and hard magnet that are combined at the nanoscale to exploit the best properties. The latter shows the improvement of the energy product based on the magnetocrystalline anisotropy. Among the various sources of magnetic anisotropy, magnetocrystalline anisotropy provides the largest anisotropy. In this manner, magnetic moment of the material may align perpendicular to the basal plane direction, providing two energy minima for the magnetization that define the uniaxial magnetic anisotropy state. Particular ferromagnetic materials showed the high moment in their ordered form, such as ordered tetragonal nitrogen martensite (α'' -Fe₁₆N₂), the L10-type equiatomic FeNi, and tetragonal L10 τ -MnAl.

This research has been focused on the latter method to develop new generation of rare-earth-free magnetic material with high-energy product. As explained in the above, to get high coercivity, it is necessary to align each magnetic moment of particle in their easy axis direction by external magnetic field, then followed by compression bulk magnet with high magnetic performance will be obtained. This such alignment only can be occurred when the particle is in a single-domain particle where each particle only composed of one domain. In a single-domain particle, all of spin will align in the same direction and the particle is uniformly magnetized with the existence of external magnetic field. Because there are no domain walls to move, the magnetization will be reversed through spin rotation rather than through the motion of domain walls, resulting in large coercivity of the nanoparticles. There are two factors which results in high coercivity of small nanoparticles: (a) spin rotation instead of domain wall motion, (b) shape anisotropy.

Rare-earth free α'' -Fe₁₆N₂ NPs, which have the highest magnetic moment among the ferromagnetic magnetic materials, are difficult to produce as single domain magnetic NPs because of its quasistable state and high reactivity. However, this NPs have high magnetic interaction among NPs and small magnetic coercivity. Therefore, the nanostructuring α'' -Fe₁₆N₂ NPs for enhancing its magnetic performance, which are important and inevitable condition for producing rare-earth-free high performance magnetic materials, is important to be investigated. The nanostructuring illustration of α'' -Fe₁₆N₂ NPs is shown in **Figure 1.9**. α'' -Fe₁₆N₂ NPs can be structured in a nanocomposite form such as film and fiber.

Nanocomposites usually comprise two or more phases of different chemical constituents or structures, with at least one of the chemicals and/or structural phases having nanometric dimensions. These nanocomposites, due to their improved physical/chemical properties, establish applications ranging from energy, sensors, biotechnology, smart materials, filtration, and regenerative medicine. These nanocomposites contribute to producing light/efficient batteries, fuel cells, and fabricating structural components fibers with high strength-to-weight ratio, lightweight sensors, as well as magnetic and fluorescent nanocomposites for efficient viewing/removing of the tumors [19].

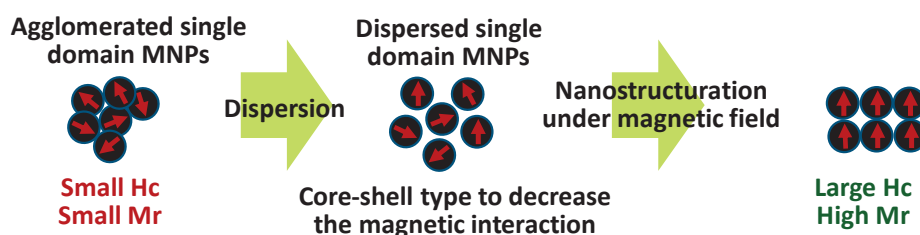


Figure 1.9 Illustration of nanostructuring of α'' -Fe₁₆N₂ nanoparticles.

1.4.1 Magnetic nanocomposite film

The research on α'' -Fe₁₆N₂ has attracted tremendous attention since Kim and Takahashi reported great invention of α'' -Fe₁₆N₂ film with magnetic moment on the order of 3.0 μ_B [20]. Subsequently, many research has been performed to investigate the magnetic properties of α'' -Fe₁₆N₂ either in film or bulk forms, whereby the Fe–N phases are grown on the Fe substrate via N doping [21, 22]. Several in-situ methods have been widely used for the preparation of α'' -Fe₁₆N₂ films that include sputtering [23-26], ion beam deposition [27], nitrogen ion implantation [28], and tempering nitride-based bulk martensite [29]. Recent studies have reported that Fe₁₆N₂ thin films can achieve high magnetic saturation M_s values [30, 31]. **Table 1.2** shows the various in-situ methods to prepare α'' -Fe₁₆N₂ films.

Even though the high magnetic performance of α'' -Fe₁₆N₂ film has been achieved, this α'' -Fe₁₆N₂ film synthesis still have limitations, i.e (1) complex synthesis methods that are usually conducted at high temperatures, (2) synthesis process is usually performed by doping N atom by flowing NH₃ and/or N₂ gases on the Fe substrate, therefore another Fe-N phase is also exist, affecting the magnetic performance, and (3) difficulty in forming singly magnetically oriented films. Therefore, alternative synthesis of α'' -Fe₁₆N₂ NPs film which can overcome those problems is more preferable.

Table 1.2 Methods of the α'' -Fe₁₆N₂ film synthesis

Method	Substrate	Film thickness	Magnetic properties	Ref
Magnetron sputtering	Silica			[32]
Facing target sputtering	GaAs		$M_s = 26.8$ kG	[33]
Plasma DC-sputtering	Al ₂ O ₃	6 μ m	$M_s = 0.35$ kG	[28]
Plasma assisted evaporation	Mo	100-300 nm	$M_s = 25$ kG	[34]
Molecular beam epitaxy	In _{0.2} Ga _{0.8} As	34-83 nm	$M_s = 28.3$ - 29.8 kG	[35]
Nitrogen ion implantation sputtering beam	Fe-MgO	50 nm - 250 nm	Magnetic moment = 2.4 μ_B /Fe	[36]

In this thesis, spin-coating was used to prepare the magnetic film using α'' -Fe₁₆N₂ NPs due to its simplicity and high processing speed. By using NPs as the raw materials resulting in the possibility for aligning their magnetic moment. The more detail investigation of structuration of α'' -Fe₁₆N₂ with aligned magnetic moment is necessary to clear this material as a candidate for high performance of permanent magnetic.

1.4.2 Magnetic nanocomposite fiber

Nanocomposite fibers consisting of magnetic nanoparticles embedded into a polymer matrix have been under intensive investigation because of their magnetic-field dependent physical properties. A large number of applications like magnetic cell separation [37], magnetic resonance imaging contrast agents [38], magnetic filters [39], magnetic sensors [40], microwave absorbers [41, 42], tissue-engineering scaffolds [43, 44], electromagnetic wave absorbers [45], magnetic catalyst [46, 47], ferroelectric photovoltaic devices [48], low frequency magnetic shielding, and magnetic hyperthermia [49] were developed based on their properties. The polymeric nanofibers containing magnetic nanoparticles combine the typical properties of a polymeric nanofiber material, i.e. high surface/volume ratio, good mechanical flexibility and high electrical resistivity, with the high magnetic susceptibility of the magnetic nanoparticles, becoming attractive materials for high-frequency electronic applications.

Among various methods to synthesize nanocomposite fiber, electrospinning showed to be a versatile and an effective synthesis method of fibers with diameters ranging from a few nanometers to several micrometers. Electrospinning has the unique ability to produce nanofibers of different materials in various fibrous assemblies. The relatively high production rate and simplicity of the setup make electrospinning highly attractive to both academia and industry. Recently, an external magnetic field was applied during electrospinning process to get an aligned nanofiber.

Several studies of the synthesis of magnetic nanocomposite fiber containing MNPs, i.e. Fe₃O₄ NPs, via magnetic-field assisted electrospinning have been reported [50-52]. Yang et al fabricated well-aligned poly (vinyl alcohol) fibers by placing two magnets at the sides of the collector during electrospinning. Wang et al used a similar magnetic-field configuration to produce aligned polyvinylpyrrolidone (PVP)/Fe₃O₄ fibers, but further plasma treatments were conducted to obtain pure Fe₃O₄ fibers with an average diameter of 200 nm. A different configuration was reported by Ajao et al [52] in which a cylindrical magnet was employed to produce well-aligned poly(ethylene oxide). However, the effects of the applied magnetic field on the fiber diameter and magnetic properties have not been thoroughly analyzed, despite the production of well-aligned fibers. Therefore, the more detail investigation on this magneto-electrospinning process is highly necessary.

Since the synthesis process of α'' -Fe₁₆N₂ NPs was conducted in gas phase with relatively high temperature, particularly on the reduction reaction, some agglomerates are usually formed. As explained in the above, to apply these particles for construction of magnetic nanocomposite materials, only well-dispersed single domain magnetic NPs are accepted. Therefore, dispersion

process after synthesis process is inevitable to form well dispersed single domain magnetic NPs.

1. 5 Objectives and Outline of the Dissertation

The main objectives of this dissertation are: detail investigation of effects of applied external magnetic field on the magnetic performance of (1) magnetic α'' -Fe₁₆N₂ NPs film (**Chapter 2 and 3**), and (2) α'' -Fe₁₆N₂ magnetic nanocomposite fiber (**Chapter 4**). To examine the enhancement of magnetic performance of the composite film and fiber, a superconducting quantum interference device magnetometer (SQUID; MPMS 5XL, Quantum Design, Japan, operated at 300 K) was used. This dissertation comprises of 5 chapters. The schematic diagram of dissertation organization is shown in **Figure 1.10**. The brief descriptions of each chapter are shown below.

Chapter 1 describes the background and the motivation of the current research. Basic theoretical explanation and review of previous researches on the α'' -Fe₁₆N₂ magnetic materials as well as an overview of the magnetic nanocomposite materials were also provided.

Synthesis of α'' -Fe₁₆N₂ NPs film via spin-coating under applied magnetic field as well as effects of these magnetic field on its magnetic performance are explained in **Chapter 2**. Core-shell single-domain α'' -Fe₁₆N₂/Al₂O₃ NPs with average size of 47 nm were synthesized by nitridation process. Due to the agglomeration, a low energy dispersion process was done to produce well-dispersed α'' -Fe₁₆N₂/Al₂O₃ NPs in toluene solvent prior to film preparation. α'' -Fe₁₆N₂ NPs film was prepared by spin coating of the well-dispersed NPs slurry on the Si substrate. An external magnetic field of 1.2 T was applied vertical to the substrate during the film formation to align the magnetic orientation of NPs followed by fixation of the NPs with resin. The SEM and XRD results showed that densely packed assemblies of the NPs were formed and aligned perpendicularly in a \sim 1 μ m film. Based on the magnetic hysteresis curve of the NPs film which is obtained from SQUID analysis, the application of the magnetic field during film formation increase the H_c and M_r values of the resulted films by 23% and 55%, respectively.

In **Chapter 3** the effect applied magnetic field strength on the magnetic properties of α'' -Fe₁₆N₂ NPs film via spin-coating are discussed in detail. The film with thickness of 1 μ m was prepared with same method as in the chapter 2. However, some external magnetic fields of strength 0, 0.6, 0.9, or 1.2 T were applied to examine the magnetic moment alignment of α'' -Fe₁₆N₂/Al₂O₃ NPs in composite films. X-ray diffraction and SQUID analyses showed the relationship between the aligned magnetic moment of the NPs and their magnetic properties;

H_c, M_r, and (BH)_{max} enhanced by 24%, 66%, and 160%, respectively, with increase in magnetic orientation of 35%. The shape of hysteresis loops of the films approached to rectangular by increasing the vertically applied magnetic field. These results were further verified by applying the magnetic field horizontally. The magnetic properties of the film were decreased by applying the magnetic field horizontal to substrate. These findings show that control of the magnetic orientation of single domains of magnetic NPs improves the magnetic performances compared with that of agglomerated magnetic NPs.

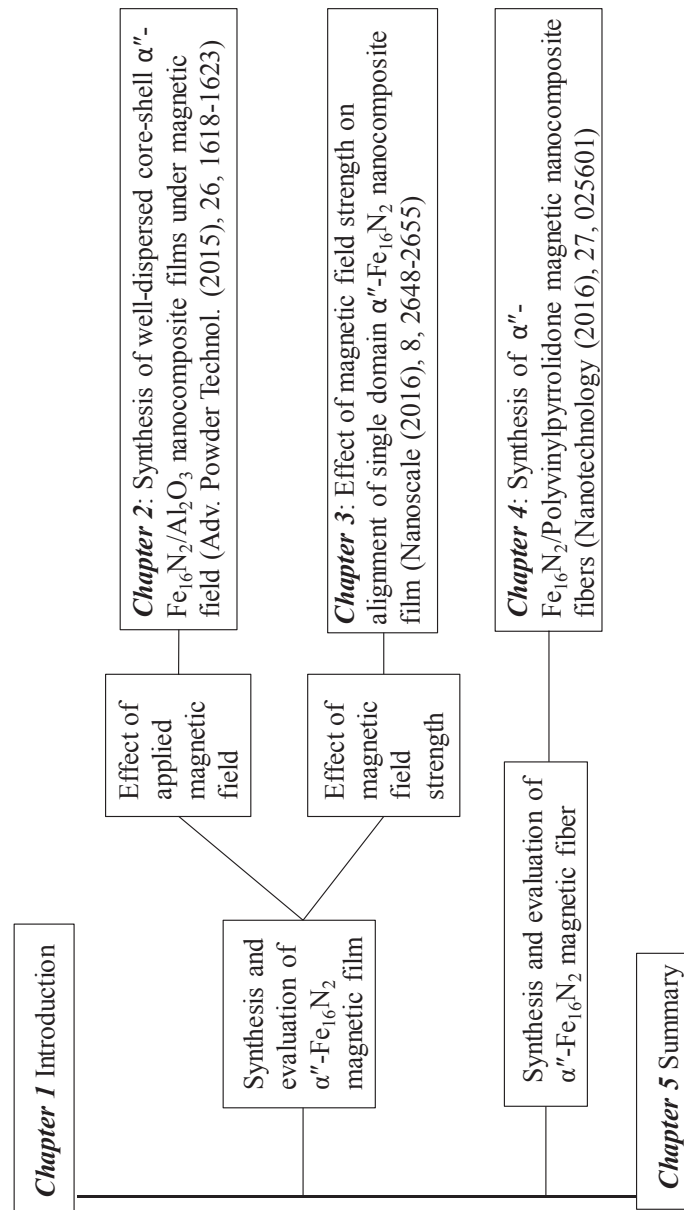


Figure 1.10 Organization and structure of chapters in the present dissertation.

According to the successfulness to synthesize well-dispersed single-domain α'' -Fe₁₆N₂ NPs film under magnetic field, the effect of applied magnetic field on diameter of

nanocomposite fiber and its magnetic performance are investigated in **Chapter 4**. Magnetic nanocomposite fibers containing α'' -Fe₁₆N₂ NPs, which is hard magnet, in polyvinylpyrrolidone (PVP) matrix were prepared via electrospinning with and without magnetic field applied of 0.1T to the spinning direction. α -Fe NPs which is soft magnet was also used to investigate the effect of NP magnetic strength on the fiber properties. These NPs were dispersed in toluene using beads-mill dispersion to prepare magnetic NPs slurry. The magnetic NP slurry was mixed with a 15 wt % of PVP dissolved in mixture of toluene and methanol with a mass ratio of 1:1 to make a ferrofluid precursor for electrospinning with two different loadings of 16.5wt% and 28.4 wt% of magnetic NPs. The ferrofluid was then electrospun with a flow rate of 2–20 $\mu\text{l min}^{-1}$ under an applied high voltage. The environment during electrospinning was kept at a temperature of (30 \pm 2) °C and a relative humidity of (30 \pm 5) %. SEM and TEM analyses results showed that the applying the magnetic field in the same direction as the electric field resulted in smaller and more uniform fiber diameters. Further, nanocomposite fibers containing α'' -Fe₁₆N₂ had smaller diameters than those containing α -Fe NPs. These magnetic-field effects on the fiber formation were explained by referring to the kinetic energy of the moving jet in the electrospinning process. In addition, magnetic hysteresis curves showed an enhancement of the Hc and Mr values by 23% and 22%, respectively.

Chapter 5 contains the summary of all chapters and direction for further investigation.

1.6 References

- [1] Lewis LH, Jiménez-Villacorta F 2013 Perspectives on permanent magnetic materials for energy conversion and power generation *Metall. Mater. Trans. A* **44** 2-20
- [2] Cros J, Viarouge P, Chalifour Y, Figueroa J 2004 A new structure of universal motor using soft magnetic composites *IEEE T. Ind. Appl.* **40** 550-7
- [3] Hayashi T, Hirono S, Tomita M, Umemura S, Delaunay JJ 1997 Magnetic thin films of cobalt nanocrystals encapsulated in graphite-like carbon *Mater. Res. Soc. Symp. Proc.* **475** 33-8
- [4] Tartaj P, del Puerto Morales M, Veintemillas-Verdaguer S, González-Carreño T, Serna CJ 2003 The preparation of magnetic nanoparticles for applications in biomedicine *J. Phys. D: Appl. Phys.* **36** R182–R97
- [5] Kim J, Park S, Lee JE, Jin SM, Lee JH, Lee IS, Yang I, Kim JS, Kim SK, Cho MH, Hyeon T 2006 Designed fabrication of multifunctional magnetic gold nanoshells and

- their application to magnetic resonance imaging and photothermal therapy *Angew. Chem.* **118** 7918-22
- [6] Scientific Reports Liu E, Yuan H, Kou Z, Wu X, Xu Q, Zhai Y, Sui Y, You B, Du J, Zhai H 2015 Investigation on spin dependent transport properties of core-shell structural Fe₃O₄/ZnS nanocomposites for spintronic application *Sci. Rep.* **5** 11164
- [7] Philip J, Laskar JM 2012 Optical properties and applications of ferrofluids—A review *J. Nanofluids* **1** 3-20
- [8] Gutfleisch O, Willard MA, Bruck E, Chen CH, Sankar SG, Liu JP 2011 Magnetic materials and devices for the 21st century: Stronger, lighter, and more energy efficient *Adv. Mater.* **23** 821-42
- [9] Bhattacharyya S 2015 Iron nitride family at reduced dimensions: A review of their synthesis protocols and structural and magnetic properties *J. Phys. Chem. C* **119** 1601-22
- [10] Wriedt HA, Gokcen NA, Nafziger RH 1987 The Fe-N (Iron-Nitrogen) system *Bulletin of Alloy Phase Diagrams* **8** 355–77
- [11] Du Marchie van Voorthuysen EH, Boerma DO, Chechenin NC 2002 Low-temperature extension of the Lehrer diagram and the iron-nitrogen phase diagram *Metall. Mater. Trans. A* **33** 2593–8
- [12] Ogawa T, Ogata Y, Gallage R, Kobayashi N, Hayashi N, Kusano Y, Yamamoto S, Kohara K, Doi M, Takano M, Takahashi M 2013 Challenge to the synthesis of α '-Fe₁₆N₂ compound nanoparticle with high saturation magnetization for rare earth free new permanent magnetic material *Appl. Phys. Express* **6** 073007
- [13] Ogi T, Nandiyanto ABD, Kiskibar Y, Iwaki T, Nakamura K, Okuyama K 2013 Facile synthesis of single-phase spherical α '-Fe₁₆N₂/Al₂O₃ core-shell nanoparticles via a gas-phase method *J. Appl. Phys.* **113** 164301
- [14] Zulhijah R, Nandiyanto ABD, Ogi T, Iwaki T, Nakamura K, Okuyama K 2014 Gas phase preparation of spherical core-shell α '-Fe₁₆N₂/SiO₂ magnetic nanoparticles *Nanoscale* **6** 6487-91
- [15] Zulhijah R, Yoshimi K, Nandiyanto ABD, Ogi T, Iwaki T, Nakamura K, Okuyama K 2014 α '-Fe₁₆N₂ phase formation of plasma-synthesized core-shell type α -Fe nanoparticles under various conditions *Adv. Powder Technol.* **25** 582-90
- [16] Zulhijah R, Nandiyanto ABD, Ogi T, Iwaki T, Nakamura K, Okuyama K 2015 Effect of oxidation on α '-Fe₁₆N₂ phase formation from plasma-synthesized spherical core-shell α -Fe/Al₂O₃ nanoparticles *J. Magn. Mater.* **381** 89-98

-
- [17] Zulhijah R, Suhendi A, Yoshimi K, Kartikowati CW, Ogi T, Iwaki T, Okuyama K 2015 Low-energy bead-mill dispersion of agglomerated core-shell α -Fe/Al₂O₃ and α' -Fe₁₆N₂/Al₂O₃ ferromagnetic nanoparticles in toluene *Langmuir* **31** 6011-9
- [18] Ogi T, Zulhijah R, Iwaki T, Okuyama K 2017 Recent progress in nanoparticle dispersion using bead mill *KONA*
- [19] Sahay R, Kumar PS, Sridhar R, Sundaramurthy J, Venugopal J, Mhaisalkar SG, Ramakrishna S 2012 Electrospun composite nanofibers and their multifaceted applications *J. Mater. Chem.* **22** 12953
- [20] Kim TK, Takahashi M 1972 New magnetic material having ultrahigh magnetic moment *Appl. Phys. Lett.* **20** 492-4
- [21] Komuro M, Kozono Y, Hanazono M, Sugita Y 1990 Epitaxial growth and magnetic properties of Fe₁₆N₂ films with high saturation magnetic flux density *J. Appl. Phys.* **67** 5126-30
- [22] Ji N, Osofsky MS, Lauter V, Allard LF, Li X, Jensen KL, Ambaye H, Lara-Curzio E, Wang JP 2011 Perpendicular magnetic anisotropy and high spin-polarization ratio in epitaxial Fe-N thin films *Phys. Rev. B* **84**
- [23] Ji N, Lauter V, Ambaye H, Wang JP 2012 Giant saturation magnetization effect in epitaxial Fe₁₆N₂ thin films grown on MgO (001) substrate *arXiv:1211.0555*
- [24] Coey JMD 2001 Magnetic materials *J. Alloys Compd.* **326** 2–6
- [25] Russak MA, Jahnes CV, Klokhholm E, Lee JW, Re ME, Webb BC 1991 Magnetic and structural characterization of sputtered FeN multilayer films *J. Appl. Phys.* **70** 6427-9
- [26] Wang X, Zheng WT, Tian HW, Yu SS, Xu W, Meng SH, He XD, Han JC, Sun CQ, Tay BK 2003 Growth, structural, and magnetic properties of iron nitride thin films deposited by DC magnetron sputtering *Appl. Surf. Sci.* **220** 30-9
- [27] Liu, Xu YH, Sanchez-Hanke C, Wang JP 2009 Discovery of localized states of Fe 3d electrons in Fe₁₆N₂ and Fe₈N films an evidence of the existence of giant saturation magnetization *arXiv:1211.0555*
- [28] Abdellateef MA, Heiden C, Lemke H, El-Hossary FM, Baerner K 2003 Magnetic properties and structure of the α' -Fe₁₆N₂ films *J. Magn. Magn. Mater.* **256** 214–20
- [29] Takahashi M, Shoji H, Takahashi H, Nashi H, Wakiyama T, Doi M, Matsui M 1994 Magnetic moment of α' -Fe₁₆N₂ films *J. Appl. Phys.* **76** 6642-7
- [30] Brewer MA, Krishnan KM, Ortiz C 1996 Epitaxial Fe₁₆N₂ films grown on Si(001) by reactive sputtering *J. Appl. Phys.* **79** 5321

-
- [31] Nakajima K, Okamoto S, Okada T 1989 Formation of ferromagnetic iron nitrides in iron thin films by high-dose nitrogen ion implantation *J. Appl. Phys.* **65** 4357-61
- [32] Kappaganthu SR, Sun Y 2003 Effect of nitrogen partial pressure and temperature on RF sputtered Fe–N films *Surf. Coat. Technol.* **167** 165-9
- [33] Ji N, Allard LF, Lara-Curzio E, Wang JP 2011 N site ordering effect on partially ordered Fe₁₆N₂ *Appl. Phys. Lett.* **98** 092506
- [34] Adachi N, Endo M, Menjo N, Okuda T 2003 Annealing effects of iron nitride thin film grown by plasma-assisted evaporation technique *J. Ceram. Soc. Jpn.* **111** 369-71
- [35] Takahashi H, Igarashi M, Kaneko A, Miyajima H, Sugita Y 1999 Perpendicular uniaxial magnetic anisotropy of Fe₁₆N₂ [001] single crystal films grown by molecular beam epitaxy *IEEE T. Magn.* **35** 2982-4
- [36] H. S, K. S 1998 Effects of film thickness on formation processes of Fe₁₆N₂ in nitrogen ion-implanted Fe films *Surf. Coat. Technol.* **103-104** 129–34
- [37] Honda H, Kawabe A, Shinkai M, Kobayashi T 1998 Development of chitosan-conjugated magnetite for magnetic cell separation *J. Ferment. Bioeng.* **86** 191–6
- [38] Lutz JF, Stiller S, Hoth A, Kaufner L, Pison U, Cartier R 2006 One-pot synthesis of PEGylated ultrasmall iron-oxide nanoparticles and their in vivo evaluation as magnetic resonance imaging contrast agents *Biomacromolecules* **7** 3132–8
- [39] Pinchuk LS, Markova LV, Gromyko YV, Markov EM, Choi US 1995 Polymeric magnetic fibrous filters *J. Mater. Process. Technol.* **55** 345-50
- [40] Epstein AJ, Miller JS 1996 Molecule- and polymer-based magnets, a new frontier *Synth. Met.* **80** 231–7
- [41] Wang T, Wang H, Chi X, Li R, Wang J 2014 Synthesis and microwave absorption properties of Fe–C nanofibers by electrospinning with disperse Fe nanoparticles parceled by carbon *Carbon* **74** 312-8
- [42] Chiscan O, Dumitru I, Postolache P, Tura V, Stancu A 2012 Electrospun PVC/Fe₃O₄ composite nanofibers for microwave absorption applications *Mater. Lett.* **68** 251-4
- [43] Hu H, Jiang W, Lan F, Zeng X, Ma S, Wu Y, Gu Z 2013 Synergic effect of magnetic nanoparticles on the electrospun aligned superparamagnetic nanofibers as a potential tissue engineering scaffold *RSC Adv.* **3** 879-86
- [44] Meng J, Xiao B, Zhang Y, Liu J, Xue H, Lei J, Kong H, Huang Y, Jin Z, Gu N, Xu H 2013 Super-paramagnetic responsive nanofibrous scaffolds under static magnetic field enhance osteogenesis for bone repair in vivo *Sci. Rep.* **3** 2655

-
- [45] Yang Y, Guo Z, Zhang H, Huang D, Gu J, Huang Z, Kang F, Alan Hatton T, Rutledge GC 2013 Electrospun magnetic carbon composite fibers: Synthesis and electromagnetic wave absorption characteristics *J. Appl. Polym. Sci.* **127** 4288-95
- [46] Korina E, Stoilova O, Manolova N, Rashkov I 2013 Poly(3-hydroxybutyrate)-based hybrid materials with photocatalytic and magnetic properties prepared by electrospinning and electrospaying *J. Mater. Sci.* **49** 2144-53
- [47] Ghasemi E, Ziyadi H, Afshar AM, Sillanpää M 2015 Iron oxide nanofibers: A new magnetic catalyst for azo dyes degradation in aqueous solution *Chem. Eng. J.* **264** 146-51
- [48] Fei L, Hu Y, Li X, Song R, Sun L, Huang H, Gu H, Chan HL, Wang Y 2015 Electrospun bismuth ferrite nanofibers for potential applications in ferroelectric photovoltaic devices *ACS Appl. Mater. Interfaces* **7** 3665-70
- [49] Kim Y-J, Ebara M, Aoyagi T 2013 A smart hyperthermia nanofiber with switchable drug release for inducing cancer apoptosis *Adv. Funct. Mater.* **23** 5753-61
- [50] Yang D, Lu B, Zhao Y, Jiang X 2007 Fabrication of aligned fibrous arrays by magnetic electrospinning *Adv. Mater.* **19** 3702-6
- [51] Wang H, Tang H, He J, Wang Q 2009 Fabrication of aligned ferrite nanofibers by magnetic-field-assisted electrospinning coupled with oxygen plasma treatment *Mater. Res. Bull.* **44** 1676-80
- [52] Ajao JA, Abiona AA, Chigome S, Fasasi AY, Osinkolu GA, Maaza M 2010 Electric-magnetic field-induced aligned electrospun poly (ethylene oxide) (PEO) nanofibers *J. Mater. Sci.* **45** 2324-9

Chapter 2

Synthesis of well-dispersed single-domain α'' -Fe₁₆N₂ nanocomposite films under magnetic field

2. 1 Introduction

Synthesis of ferromagnetic nanoparticles (NPs) with a single-domain has attracted much attention for the formation of bulk magnet [1-4]. Recent reports have shown that these ferromagnetic NPs with single-domain, by magnetically aligned assembly, will give higher magnetic performance than that of large magnetic NPs with many domains [5-8]. However, most of these ferromagnetic NPs with the highest magnetocrystalline anisotropy usually composed of rare-earth elements, such as Nd, Sm, and Dy [8-11]. Therefore, synthesis of single domain ferromagnetic NPs without rare-earth component and alignment of their magnetic moment are still become a challenge in the magnet development.

α'' -Fe₁₆N₂ NPs have been reported as the ferromagnetic NPs with the highest magnetic moment and uniaxial magnetic anisotropy among ferromagnetic NPs [12]. Moreover, due to these excellent magnetic properties, these α'' -Fe₁₆N₂ NPs have a great potential for the rare-earth-free magnetic material applications. However, compared to the rare-earth magnetic materials, such as Nd₂Fe₁₄B and SmCo₅, these α'' -Fe₁₆N₂ NPs still have relatively low magnetic coercivity value (H_c) and more studies are still necessary to enhance their H_c value. Therefore, synthesis of single domain α'' -Fe₁₆N₂ NPs and alignment of their magnetic moment may become a prospective method to increase H_c value of α'' -Fe₁₆N₂ NPs.

However, since this α'' -Fe₁₆N₂ NP is a hard magnet material, these particles will easy to agglomerate during the preparation process, for that it will be difficult to synthesize α'' -Fe₁₆N₂ NPs with a single-domain and in well-disperse condition. Thus, dispersion process after NPs synthesis will be necessary prior to further magnetic alignment process.

Recently, our group successfully synthesized spherical core–shell typed α'' -Fe₁₆N₂ NPs via a gas phase method using α -Fe, and Al₂O₃ or SiO₂ as the core and shell, respectively [13-15]. The synthesized core–shell magnetic NPs primarily constituted single phase α'' -Fe₁₆N₂ and had a relatively high magnetic performance without any hard aggregation of the NPs observed. The core–shell α'' -Fe₁₆N₂/Al₂O₃ NPs has been bead-milled to break up aggregates into the primary NPs with a single-domain.

Based on this successfulness to prepare well-dispersed single-domain α'' -Fe₁₆N₂ NPs, as the continuation for the next step process, the magnetic alignment process is performed in a film form. Preparation of these α'' -Fe₁₆N₂ NPs in the film form are selected and more preferable to demonstrate the magnetic alignment process, because in the film form, the particle will be easier to be aligned in a single direction rather than in the bulk form. Therefore, the evaluation on this magnetic alignment will be easier. Moreover, the preparation of these α'' -Fe₁₆N₂ NPs in the film form allow these particles to be applied in many applications, such as magnetic sensor, magnetic recording media, and especially for the construction of rare-earth-free bulk magnetic material with high magnetic performance. In addition, the formation of α'' -Fe₁₆N₂ NPs in the film form has not been reported elsewhere.

In this research, the formation of α'' -Fe₁₆N₂ NPs composite films using α'' -Fe₁₆N₂ NPs is reported. Core-shell single-domain α'' -Fe₁₆N₂/Al₂O₃ NPs were used as a basic material. For a model process, spin-coating method was used due to its simplicity and high processing speed. An external magnetic field was applied during spin-coating to align the magnetic moment of the assembled NPs. The evaluated magnetic performance of the prepared α'' -Fe₁₆N₂ NPs films demonstrates the potential of magnetic NPs to be used as a base material for magnetically aligned film. This study also creates possibilities for the construction of bulk magnetic materials from α'' -Fe₁₆N₂ NPs.

2. 2 Experimental

2.2.1 Preparation of raw materials

Core-shell single-domain α -Fe/Al₂O₃ magnetic NPs used as raw material in this research was prepared by one-step radio-frequency thermal plasma process. This synthesis was explained in our previous reports [16]. To synthesize core-shell α -Fe/Al₂O₃ magnetic NPs, precursors containing pentacarbonyl iron (purity 99.5%, BASF) and alumina (1 μ m, purity 99.9%, Kojundo Chem. Lab. Co. Ltd. was used. The produced core-shell α -Fe/Al₂O₃ NPs were then stored in a glove box with N₂ environment. The raw materials such as epoxy resin were purchased from Sigma Aldrich (China) and toluene (99.95%) was purchased from Kanto Chemicals (Japan). These raw materials were used without further treatment or purification.

2.2.2 Preparation of magnetic NPs film

The detailed routes on magnetic alignment of core-shell single-domain α'' -Fe₁₆N₂/Al₂O₃ NPs in the film form are shown in **Figure 2.1**. First, α -Fe/Al₂O₃ NPs were synthesized by one-

step radio-frequency thermal plasma process. Then, the plasma synthesized $\alpha\text{-Fe}/\text{Al}_2\text{O}_3$ NPs were subjected to hydrogen reduction reaction at 275 °C for 1.5 h and subsequent nitridation process by flowing NH_3 gas at 145 °C for 15 h in a fluidized bed reactor similarly to the procedure described in our previous studies [13, 16]. The synthesized $\alpha''\text{-Fe}_{16}\text{N}_2/\text{Al}_2\text{O}_3$ NPs were then stored in toluene as a slurry for passivation. The $\alpha''\text{-Fe}_{16}\text{N}_2/\text{Al}_2\text{O}_3$ NPs slurry was fed into bead-mill dispersion process employing zirconia beads (diameter: 30 μm) to obtain dispersed $\alpha''\text{-Fe}_{16}\text{N}_2/\text{Al}_2\text{O}_3$ NPs slurry as explained in our previous report [17]. The obtained dispersed $\alpha''\text{-Fe}_{16}\text{N}_2/\text{Al}_2\text{O}_3$ NPs slurry was purified further from the excess dispersants and broken particles by centrifugation (Himac CR 22G; Hitachi, Japan). The purified slurry was then concentrated by mean of rotary evaporation (Buchi Rotavapor R-200, Switzerland). For the film formation process, the concentrated $\alpha''\text{-Fe}_{16}\text{N}_2/\text{Al}_2\text{O}_3$ NPs slurry was dropped onto a Si wafer and spin coated using dual speed [18] by a spin coater (Mikasa 1H-D7, Japan) at 200 and 1000 rpm subsequently. During film formation, a magnetic field of 1.2 T was applied vertically to the film using a magnetic circuit that was set up between the film surface and bottom of the Si wafer until the film was dried. Furthermore, adhesive cyanoacrylate resin was embedded into the film to fix the magnetic moment alignment of the $\alpha''\text{-Fe}_{16}\text{N}_2/\text{Al}_2\text{O}_3$ NPs following by removal of the applied magnetic field

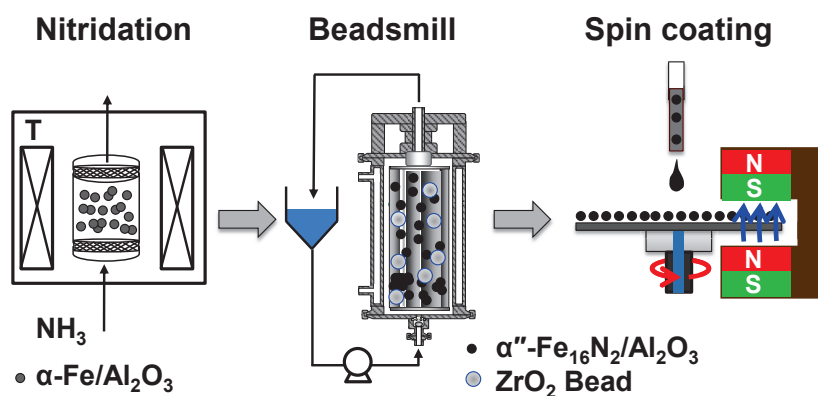


Figure 2.1. Schematic illustration of the preparation process of magnetically aligned core-shell single-domain $\alpha''\text{-Fe}_{16}\text{N}_2/\text{Al}_2\text{O}_3$ NPs films.

2.2.3 Characterization

The particle size distribution during bead-mill dispersion was evaluated by dynamic light scattering (DLS; HPPS-5001, Malvern Instruments Ltd., UK). The morphology of the $\alpha''\text{-Fe}_{16}\text{N}_2/\text{Al}_2\text{O}_3$ NPs was observed using a scanning electron microscope (SEM; Hitachi S-5000, Japan) and a transmission electron microscope (TEM; JEM-3000F, JEOL, Japan).

Characterization of the elemental composition of the core and shell of the particles was conducted using a scanning transmission electron microscope coupled with electron energy loss spectroscope (STEM-EELS; HD- 2700, Hitachi, Japan), using an operating voltage of 200 kV and beam size of 0.2 nm, and elemental analysis (776 ENFINA 1000, Gatan). The crystalline structure of the NPs was examined using X-ray diffraction (XRD; D2 Phaser, Bruker, Germany). The magnetic properties were evaluated on a superconducting quantum interference device (SQUID, Quantum Design, USA). Magnetization was measured as a function of applied field from 1 to 50 kOe at 300 K. The magnetic hysteresis loops were measured using the magneto-optic Kerr effect (MOKE, BH-620LP, Neoark, Japan) technique.

2.3 Results and discussion

2.3.1 Physicochemical properties of α'' -Fe₁₆N₂/Al₂O₃ NPs

The physicochemical properties of the α'' -Fe₁₆N₂/Al₂O₃ NPs prepared by nitridation of plasma synthesized α -Fe/Al₂O₃ NPs are shown in **Figure 2.2**. As observed from the SEM image in **Figure 2.2** (a) and bottom-left inset of **Figure 2.2** (a), respectively, the as-prepared α'' -Fe₁₆N₂/Al₂O₃ NPs are slightly agglomerated without significant sintering and featured average particle size and shell thickness of 47 nm and ~4.5 nm, respectively. The obtained particle size is appropriate for permanent magnet applications and the presence of the thin shell decreases magnetic lateral interactions among the particles, particularly during the magnetically aligned film preparation. EELS analysis, **Figure 2.2** (b), shows that the core is iron and the shell consists of Fe and Al, thus confirming that the shell is composed of aluminum oxide and iron oxide as amorphous state in the surface of iron core due to the passivation of iron as reported in our previous study [15].

Owing to the agglomerated state of the as-prepared α'' -Fe₁₆N₂/Al₂O₃ NPs, dispersion of the NPs to break down the agglomerates is required prior to film preparation. Low-energy bead-mill dispersion has been well investigated in our previous studies [17, 19, 20] to disperse agglomerated and aggregated particles into primary particles without changing the particle properties. The properties of α'' -Fe₁₆N₂/Al₂O₃ NPs after bead-mill dispersion is shown in **Figure 2.2** (c) and (d). TEM image as shown in **Figure 2.2** (c) shows that after dispersion, non-agglomerated particles without any necking among the particles were obtained. XRD results confirm that the crystal properties of the α'' -Fe₁₆N₂/Al₂O₃ NPs after bead-mill dispersion did not significantly change relative to those of the particles before dispersion as shown in **Figure**

2.2 (d). These results confirm that the α'' -Fe₁₆N₂/Al₂O₃ NPs are in well-dispersed state prior to their alignment of magnetic moment during film synthesis.

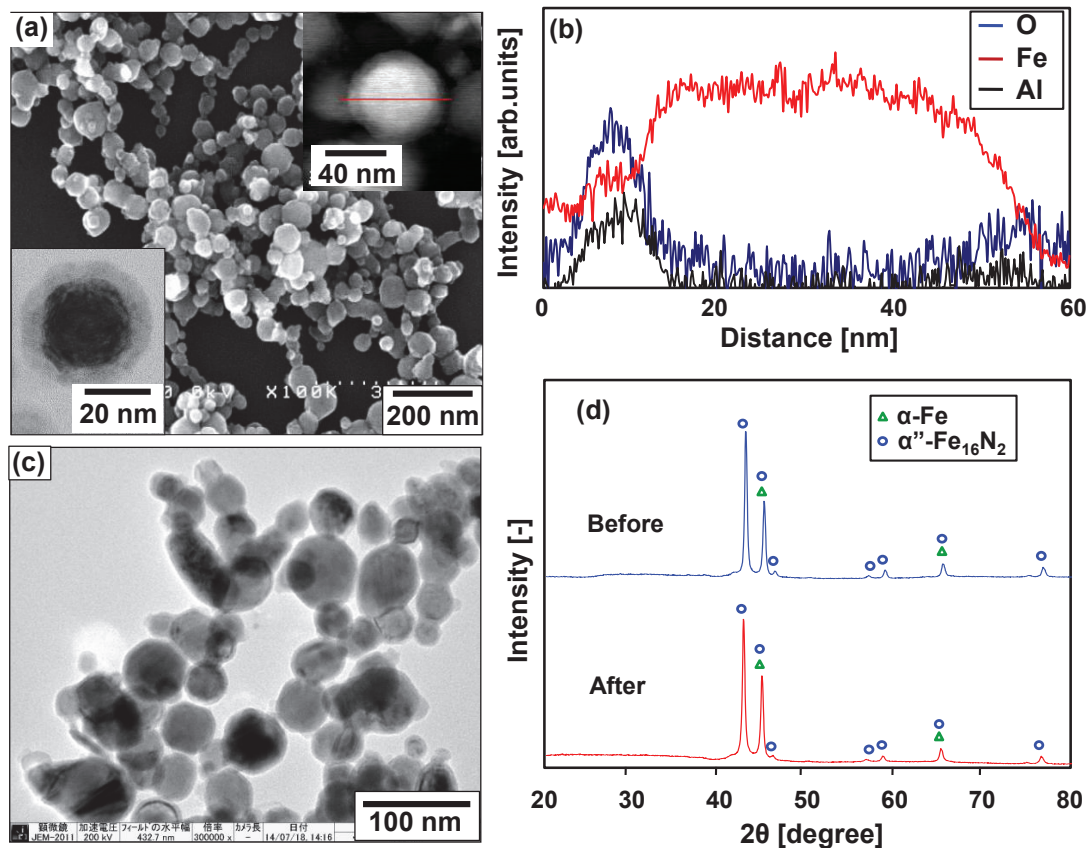


Figure 2.2. Physicochemical properties of as-prepared and dispersed core-shell α'' -Fe₁₆N₂/Al₂O₃ NPs. (a) SEM image and (b) EELS analysis of as-prepared NPs. (c) TEM image of dispersed NPs. (d) XRD pattern of as-prepared and dispersed NPs. The insets in (a) show cross sectional TEM images of the particle. The red line in the top-right inset of (a) is the scanned range for the EELS line analysis.

2.3.2 Structure of magnetically aligned film

Figure 2.3 shows the SEM images of the surface and cross-section of the spin-coated film constituting the α'' -Fe₁₆N₂/Al₂O₃ NPs. **Figure 2.3** (a) shows a smooth and dense-packed α'' -Fe₁₆N₂/Al₂O₃ NPs film with a thickness of $\sim 1 \mu\text{m}$. The dense-packing of the α'' -Fe₁₆N₂/Al₂O₃ NPs in the film was due to the well-dispersed state of the NPs. When magnetic field was applied to the film, the film surface was turned into spikes-like shape, where this pattern is generally found in ferrofluid under magnetic field [21]. Resin was immersed over the film surface to maintain the NPs arrangement in the film as shown in **Figure 2.3** (b). The application of resin may affect the formation of spikey shapes on the film surface, in which the shape is not

completely same as in the ferrofluids. Magnetic field applied on the film caused the particles to be distributed into groups of NPs on the substrate. However, no strongly agglomerated particles in the group were observed. These results confirm that the dispersion process prior to film preparation plays an important role in the film formation.

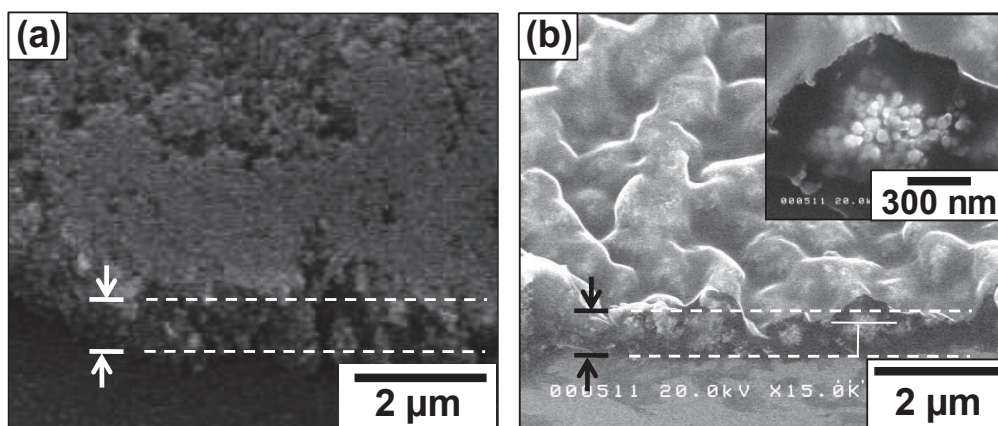


Figure 2.3. SEM images of cross section of the core-shell α'' - $\text{Fe}_{16}\text{N}_2/\text{Al}_2\text{O}_3$ NPs spin-coated film viewed at a tilt angle of 40° : (a) without resin and no applied magnetic field and (b) with resin under applied magnetic field. Inset in (b) shows the cross section of the oriented film. Dashed lines show the average film thickness.

This phenomenon can be illustrated in **Figure 2.4**. In the case of no magnetic field applied, the dispersed single domain magnetic NPs are easily interact each other forming dense packed NPs film. When the magnetic field applied (out of plane direction) during the spin coating process is higher than lateral magnetic interaction, the single domain magnetic NPs are decoupled forming separated clumps of magnetic domains. When the magnetic field applied is removed, the aligned magnetic NPs are in unstable state and easily coupled each other forming the original flat surface shape. Therefore, to maintain the magnetic alignment, the movement of the magnetic NPs should be prevented by the adhesive resin (as shown in **Figure 2.3** (b)).

Films prepared with and without magnetic field during the spin coating process were expected to have different degree of alignment. To evaluate the particle alignment of the prepared magnetic film, XRD analysis was conducted. **Figure 2.5** shows the XRD patterns of the randomly and vertically aligned α'' - $\text{Fe}_{16}\text{N}_2/\text{Al}_2\text{O}_3$ film referring to the films prepared without and with the existence of magnetic field during spin coating process, respectively. Both XRD pattern of the films were compared to those of the NPs form. High intensity peak of Si (004) substrate was observed for both films and were excluded from the comparison.

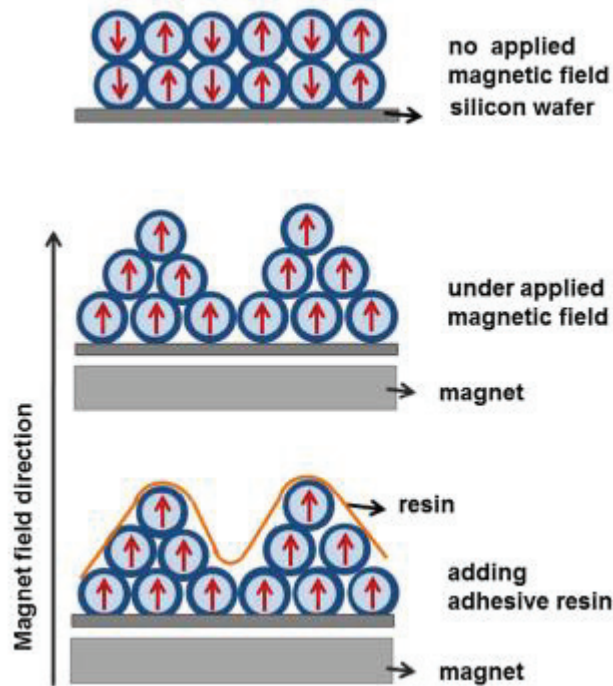


Figure 2.4. Illustration of magnetic particle direction in several conditions: no applied magnetic field, under magnetic field and after fixation using adhesive resin.

By comparing the XRD pattern of the randomly aligned $\alpha''\text{-Fe}_{16}\text{N}_2/\text{Al}_2\text{O}_3$ films to the powder (**Figure 2.2** (d)) form, it can be shown that the (103), (213) and (004) peaks vanish while other (202), (220), and (400) peaks remain. This result shows that in the film form, the $\alpha''\text{-Fe}_{16}\text{N}_2/\text{Al}_2\text{O}_3$ NPs are tend to align in the in-plane direction. When comparing the XRD pattern of the vertically with the randomly aligned films, the (400) peak disappears, while (004) peak appears. Moreover, the (220) peak decreases significantly while the (224) peak increases. These results suggest that in the vertically aligned film, the magnetic moment of the NPs tend to align in the out of plane direction. However, the remains of (202), (220), and (224) peaks showed that not all the particles are aligned completely in the vertical orientation.

From these XRD peaks, the degree of particle orientation can also be estimated. The Lotgering factor (LF) has been proven to be of good use for the evaluation of particle orientation due to the simplicity and easy in calculation. The LF is calculated from the intensities of XRD peaks with the conventional $2\theta/\theta$ scan mode, and is defined as the following equation:

$$\text{LF} = \frac{p - p_0}{1 - P_0} \quad (2.1)$$

where LF is Lotgering factor, p is the fraction of the summation of the peak intensities corresponding to the preferred alignment axis to that of the summation of all diffraction peaks in particle-aligned materials. p_0 is p of a material with a random particle distribution [22].

Using the above calculation, LF value is 0.31. The results confirmed that not all particles were vertically oriented, therefore stronger magnetic field is necessary to increase the orientation of the particles in the film. Further study on the effects of magnetic field strength will be investigated in our future work.

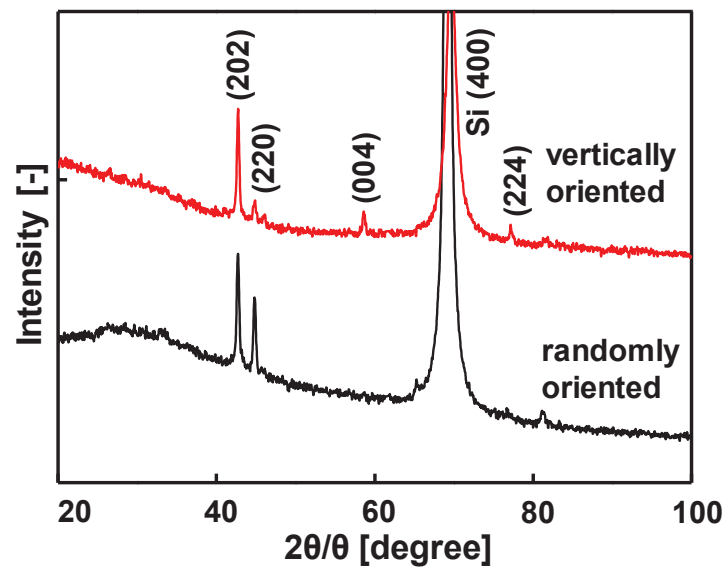


Figure 2.5. XRD patterns of vertically and randomly oriented of the α'' - $\text{Fe}_{16}\text{N}_2/\text{Al}_2\text{O}_3$ magnetic NPs films.

2.3.3 Magnetic properties of magnetically aligned film

Applying a magnetic field to the film enables control over the alignment of the magnetic moment of NPs in the film that can increase the magnetic anisotropic properties. Kerr effect and SQUID analyses were conducted to evaluate the magnetic performance of the prepared α'' - $\text{Fe}_{16}\text{N}_2/\text{Al}_2\text{O}_3$ NPs films. **Figure 2.6** shows the hysteresis curves obtained by Kerr effect measurements of the spin-coated α'' - $\text{Fe}_{16}\text{N}_2/\text{Al}_2\text{O}_3$ NPs films prepared under the presence and absence of an applied magnetic field of 1.2 T at 300 K. The results showed that both films had the same H_c value of ~ 3.5 kOe. However, the Kerr rotation values were different; the out-of-plane-oriented film had larger Kerr rotation angles when compared with the randomly oriented film. These results show that alignment of the magnetic moment of the α'' - $\text{Fe}_{16}\text{N}_2/\text{Al}_2\text{O}_3$ NPs in the film increases the anisotropy of the film.

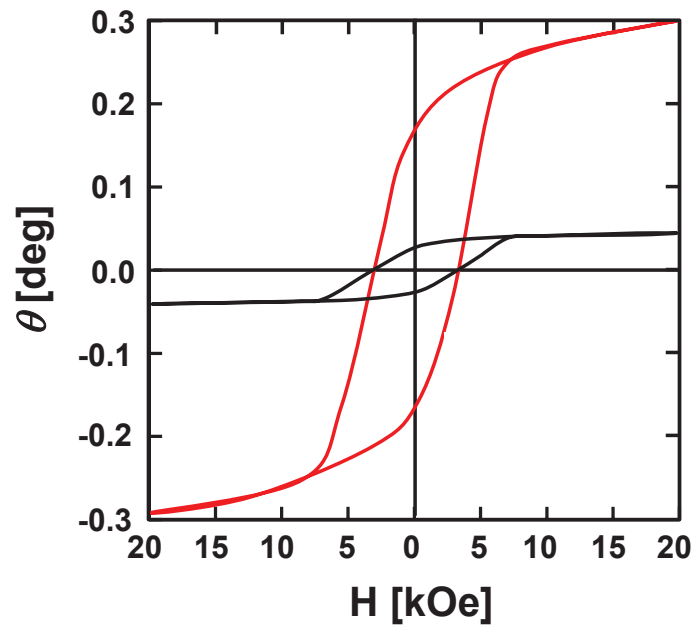


Figure 2.6 Magneto-optic Kerr effect analysis of the core-shell α'' -Fe₁₆N₂/Al₂O₃ NPs films. The red and black curves show the hysteresis of the films prepared under the presence and absence of an applied magnetic field, respectively.

Figure 2.7 shows the magnetic property of the randomly and vertically oriented films obtained by SQUID analysis. In each M-H loop, magnetization is normalized by the saturation magnetization (M_s) value of the film. The M_s value was determined by simple extrapolation of the M value to $1/H_{ex}^2 \rightarrow 0$, where H_{ex} refers to the applied field. The M_s values of the randomly and vertically aligned films were 651 and 721 emu/cc, respectively, corresponding to 0.82 and 0.91 T, respectively by removing the resin contribution and estimating the occupancy of the α'' -Fe₁₆N₂/Al₂O₃ NPs inside the film [23]. M_s value for the vertically oriented film was higher than the randomly oriented. This may be due to the estimation of the dimension of the film. H_c value of the vertically oriented film was 2.7 kOe that was higher than the randomly oriented film (2.2 kOe), showing that alignment of the magnetic moment of the particle in the film significantly enhanced the magnetocrystalline anisotropy of the film, increasing their magnetic performance. This result was also confirmed by M_r/M_s values: randomly and vertically oriented films were 0.29 and 0.45, respectively.

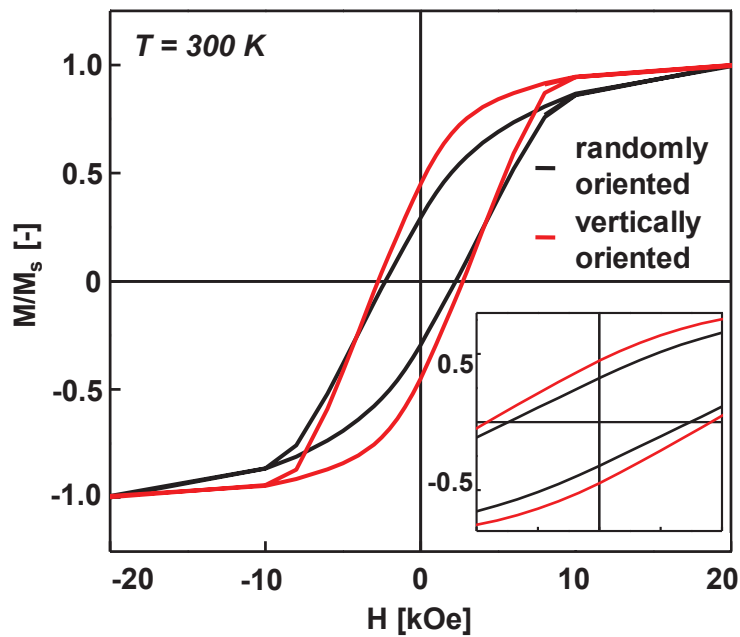


Figure 2.7 Hysteresis loops of the core-shell $\alpha''\text{-Fe}_{16}\text{N}_2/\text{Al}_2\text{O}_3$ NPs films measured on a SQUID magnetometer at 300 K for randomly and vertically oriented films.

2. 4 Conclusion

Nanostructured spherical core-shell single-domain $\alpha''\text{-Fe}_{16}\text{N}_2/\text{Al}_2\text{O}_3$ NPs films were prepared by spin-coating of well-dispersed core-shell $\alpha''\text{-Fe}_{16}\text{N}_2/\text{Al}_2\text{O}_3$ NPs in toluene. The spherical $\alpha''\text{-Fe}_{16}\text{N}_2$ NPs were aligned under an applied magnetic field of 1.2 T during spin-coating. XRD results confirmed the successful orientation of the $\alpha''\text{-Fe}_{16}\text{N}_2/\text{Al}_2\text{O}_3$ NPs in the film. Kerr effect evaluation showed that the spin-coated $\alpha''\text{-Fe}_{16}\text{N}_2/\text{Al}_2\text{O}_3$ NPs had a higher H_c of 3.5 kOe than the as-prepared $\alpha''\text{-Fe}_{16}\text{N}_2/\text{Al}_2\text{O}_3$ NPs (2.5 kOe) [13]. SQUID analysis shows the increase in H_c and M_r of 22.7% and 55.2%, respectively, after the application of magnetic field. This result shows that the $\alpha''\text{-Fe}_{16}\text{N}_2/\text{Al}_2\text{O}_3$ NPs have potential for the construction of bulk magnetic materials using $\alpha''\text{-Fe}_{16}\text{N}_2$ NPs

2. 5 References

- [1] Poudyal N, Liu JP 2013 Advances in nanostructured permanent magnets research *J. Phys. D: Appl. Phys.* **46** 043001
- [2] Yue M, Li Y, Wu Q, Liu WQ 2014 Bulk nanostructural permanent magnetic materials *Rev. Nanosci. Nanotechnol.* **3** 276-88
- [3] Sellmyer DJ 2002 Strong magnets by self-assembly *Nature* **420** 374-5

- [4] Balamurugan B, Das B, Mukherjee P, Sellmyer DJ 2014 Development of nanoparticle-based permanent-magnet materials challenges and advances *REPM* 429–32
- [5] Balamurugan B, Das B, Shah VR, Skomski R, Li XZ, Sellmyer DJ 2012 Assembly of uniaxially aligned rare-earth-free nanomagnets *Appl. Phys. Lett.* **101** 122407
- [6] Figueroa AI, Bartolome' J, Bartolome' F, Garc'ia LM, Deranlot C, Petroff F 2012 Perpendicular magnetic anisotropy of Co–Pt and Co–Pd granular films *Journal de Ciencia e Ingenieria* **4** 49 - 53
- [7] Eloi JC, Okuda M, Carreira SC, Schwarzacher W, Correia MJ, Figueiredo W 2014 Effective energy barrier distributions for random and aligned magnetic nanoparticles *J. Phys.: Condens. Matter* **26** 146006
- [8] Liu WQ, Zuo JH, Yue M, Cui ZZ, Zhang DT, Zhang JX, Zhang PY, Ge HL, Guo ZH, Li W 2011 Structure and magnetic properties of bulk anisotropic SmCo₅/ α -Fe nanocomposite permanent magnets with different α -Fe content *J. Appl. Phys.* **109** 07A741
- [9] Yue M, Pan R, Liu RM, Liu WQ, Zhang DT, Zhang JX, Zhang XF, Guo ZH, Li W 2012 Crystallographic alignment evolution and magnetic properties of NdFeB nanoflakes prepared by surfactant-assisted ball milling *J. Appl. Phys.* **111** 07A732
- [10] Hirosawa S 2015 Current status of research and development toward permanent magnets free from critical elements *J. Magn. Soc. Jpn.* **39** 85-95
- [11] He S, Jing Y, Wang JP 2013 Direct synthesis of large size ferromagnetic SmCo₅ nanoparticles by a gas-phase condensation method *J. Appl. Phys.* **113** 134310
- [12] Ogawa T, Ogata Y, Gallage R, Kobayashi N, Hayashi N, Kusano Y, Yamamoto S, Kohara K, Doi M, Takano M, Takahashi M 2013 Challenge to the synthesis of α "-Fe₁₆N₂ compound nanoparticle with high saturation magnetization for rare earth free new permanent magnetic material *Appl. Phys. Express* **6** 073007
- [13] Ogi T, Nandiyanto ABD, Kusakibaru Y, Iwaki T, Nakamura K, Okuyama K 2013 Facile synthesis of single-phase spherical α "-Fe₁₆N₂/Al₂O₃ core-shell nanoparticles via a gas-phase method *J. Appl. Phys.* **113** 164301
- [14] Zulhijah R, Nandiyanto ABD, Ogi T, Iwaki T, Nakamura K, Okuyama K 2014 Gas phase preparation of spherical core-shell α "-Fe₁₆N₂/SiO₂ magnetic nanoparticles *Nanoscale* **6** 6487-91

- [15] Zulhijah R, Nandiyanto ABD, Ogi T, Iwaki T, Nakamura K, Okuyama K 2015 Effect of oxidation on α'' -Fe₁₆N₂ phase formation from plasma-synthesized spherical core-shell α -Fe/Al₂O₃ nanoparticles *J. Magn. Magn. Mater.* **381** 89-98
- [16] Zulhijah R, Yoshimi K, Nandiyanto ABD, Ogi T, Iwaki T, Nakamura K, Okuyama K 2014 α'' -Fe₁₆N₂ phase formation of plasma-synthesized core-shell type α -Fe nanoparticles under various conditions *Adv. Powder Technol.* **25** 582-90
- [17] Zulhijah R, Suhendi A, Yoshimi K, Kartikowati CW, Ogi T, Iwaki T, Okuyama K 2015 Low-energy bead-mill dispersion of agglomerated core-shell α -Fe/Al₂O₃ and α'' -Fe₁₆N₂/Al₂O₃ ferromagnetic nanoparticles in toluene *Langmuir* **31** 6011-9
- [18] Nandiyanto ABD, Ogi T, Iskandar F, Okuyama K 2011 Highly ordered porous monolayer generation by dual-speed spin-coating with colloidal templates *Chem. Eng. J.* **167** 409-15
- [19] Joni IM, Ogi T, Iwaki T, Okuyama K 2013 Synthesis of a colorless suspension of TiO₂ nanoparticles by nitrogen doping and the bead-mill dispersion process *Ind. Eng. Chem. Res.* **52** 547-55
- [20] Tahara T, Imajyo Y, Nandiyanto ABD, Ogi T, Iwaki T, Okuyama K 2014 Low-energy bead-milling dispersions of rod-type titania nanoparticles and their optical properties *Adv. Powder Technol.* **25** 1492-9
- [21] Clark NA 2013 Soft-matter physics: Ferromagnetic ferrofluids *Nature* **504** 229–30
- [22] Furushima R, Tanaka S, Kato Z, Uematsu K 2010 Orientation distribution–Lotgering factor relationship in a polycrystalline material—as an example of bismuth titanate prepared by a magnetic field *J. Ceram. Soc. Jpn.* **118** 921-6
- [23] Martin CL, Bouvard D 2004 Isostatic compaction of bimodal powder mixtures and composites *Int. J. Mech. Sci.* **46** 907-27

Chapter 3

Effect of magnetic field strength on the alignment of single domain α'' -Fe₁₆N₂ nanocomposite films

3.1 Introduction

Ferromagnetic FePt nanoparticles (NPs) ranging in size from single to several tens of nanometers and SmCo, NdFeB, and α'' -Fe₁₆N₂ NPs have been widely studied, and much research has focused on the functionalization of NP assemblies [1-4]. Such magnetic NP assemblies are expected to provide high-performance magnetic materials for practical applications in new nanotechnologies such as ultrahigh-density recording media, high-performance nanocomposite bulk magnets, biomedical materials, spintronic devices, and environmentally friendly technologies [5-12]. Different applications require NP assemblies with different magnetic properties. Precise control of the magnetic properties of NP assemblies is therefore highly necessary [13]. Control of their magnetic properties enables NP assemblies to be used in a wider range of advanced applications.

Recently, rare-earth-free high-magnetic-moment NPs, namely single-domain ferromagnetic spherical α'' -Fe₁₆N₂ NPs have been successfully synthesized [2, 14-16]. As rare-earth-free magnetic material, α'' -Fe₁₆N₂ NPs have a theoretical BM product of 130 MGOe. These implies that this NPs are a prospective magnetic material, although the present H_c value is not as high as those of the rare-earth materials. The α'' -Fe₁₆N₂ phase was formed by nitriding core-shell α -Fe NPs that were prepared directly using a plasma method. It was expected that assembled magnetic films or bulk materials with higher magnetizations and coercivities, in which α'' -Fe₁₆N₂ NPs are isolated as single-domain particles covered with non-magnetic materials such as Al₂O₃ or SiO₂, could be obtained.

Several methods have been widely used for the preparation of α'' -Fe₁₆N₂ films, including sputtering, ion beam deposition, nitrogen-ion implantation, tempering nitride-based bulk martensite, and dip coating [17, 18]. However it is difficult to form a pure α'' -Fe₁₆N₂ phase (other Fe-N phases are present, affecting the magnetic properties) and to control the magnetic moment orientation of the film to improve the magnetic performance. Control of the magnetic moment orientation, simply called the magnetic moment, of magnetic NP assemblies is therefore still a challenge and crucial for the development of new nanostructured magnets.

Our group successfully prepared a ferrofluid of well-dispersed core-shell α'' -Fe₁₆N₂/Al₂O₃ NPs by a low-energy bead-mill dispersion method [19]. A new route to form a ferromagnetic film from rare-earth-free well-dispersed α'' -Fe₁₆N₂ NPs with the presence and absence of an applied magnetic field was established [20]. The applied magnetic field aligned the easy c-axis and magnetic moment of the NPs, resulting in the enhancement of the magnetic performance of the film. The magnetic remanence ratio (Mr/Ms) and coercivity (Hc) increased by 55.2% and 24%, respectively upon the application of a 1.2 T magnetic field. However, the effects of the magnetic field on the magnetic moment alignment of the NP films and their magnetic properties were not examined. As a continuation of our previous studies [20], we have focused on the control of the magnetic moment alignment during the synthesis of α'' -Fe₁₆N₂ films using well-dispersed α'' -Fe₁₆N₂ NPs and analyzed the relationship between the aligned magnetic moment of the NPs and their magnetic properties, using newly prepared α'' -Fe₁₆N₂ NPs.

In this research, α'' -Fe₁₆N₂ NPs films were prepared by spin-coating, using the same method as in our previous study [20]. Magnets with various magnetic field strengths up to 1.2 T were applied during the film formation to align the magnetic moment of the assembled NPs in the same direction before fixing the NPs in the film with epoxy resin binder. The magnetic properties such as the magnetic coercivity (Hc), magnetic remanence (Mr), maximum energy product [(BH)max], and anisotropic magnetic field (Hk) of the prepared α'' -Fe₁₆N₂ NP films show that the control of the magnetic moment alignment improves the performance of the resulting magnetic materials. The magnetic properties of the α'' -Fe₁₆N₂ NP films show the potential for the nanostructuring of bulk magnetic materials with tunable magnetic properties.

3. 2 Experimental

3.2.1 Preparation of raw materials

The synthesis of ferromagnetic core-shell single-domain α'' -Fe₁₆N₂/Al₂O₃ NPs by the nitridation of plasma synthesized core-shell single-domain α -Fe/Al₂O₃ NPs was described in our previous report [2, 14, 16]. The raw materials such as epoxy resin were purchased from Sigma Aldrich (China) and toluene (99.95%) was purchased from Kanto Chemicals (Japan). These raw materials were used without further treatment or purification.

3.2.2 Preparation of magnetically aligned films

A concentrated ferrofluid containing α'' -Fe₁₆N₂/Al₂O₃ NPs dispersed in toluene (59 wt%), prepared by low-energy bead-mill dispersion [19], was mixed with epoxy resin (3,4-

epoxycyclohexylmethyl 3,4-epoxycyclohexanecarboxylate) as an NP binder, in a mass ratio of 1 : 1. The mixed solution was dropped onto a silica (Si) wafer and coated using a spin-coater (Mikasa 1H-D7, Japan) at 300 and 1000 rpm for 30 and 10 s, respectively, as previously described [20]. After the formation of the thin film on the Si wafer, magnetic fields of strength 0, 0.6, 0.9, and 1.2 T were applied before the toluene evaporated from the coated film. The magnetically aligned NP film was dried and completely fixed with the resin, and then the magnetic field was removed. Details of the preparation of the magnetically aligned core-shell α'' - $\text{Fe}_{16}\text{N}_2/\text{Al}_2\text{O}_3$ NP film are shown in **Figure 3.1**, and details of the applied magnetic fields used in preparing the various samples are listed in Table 3.1.

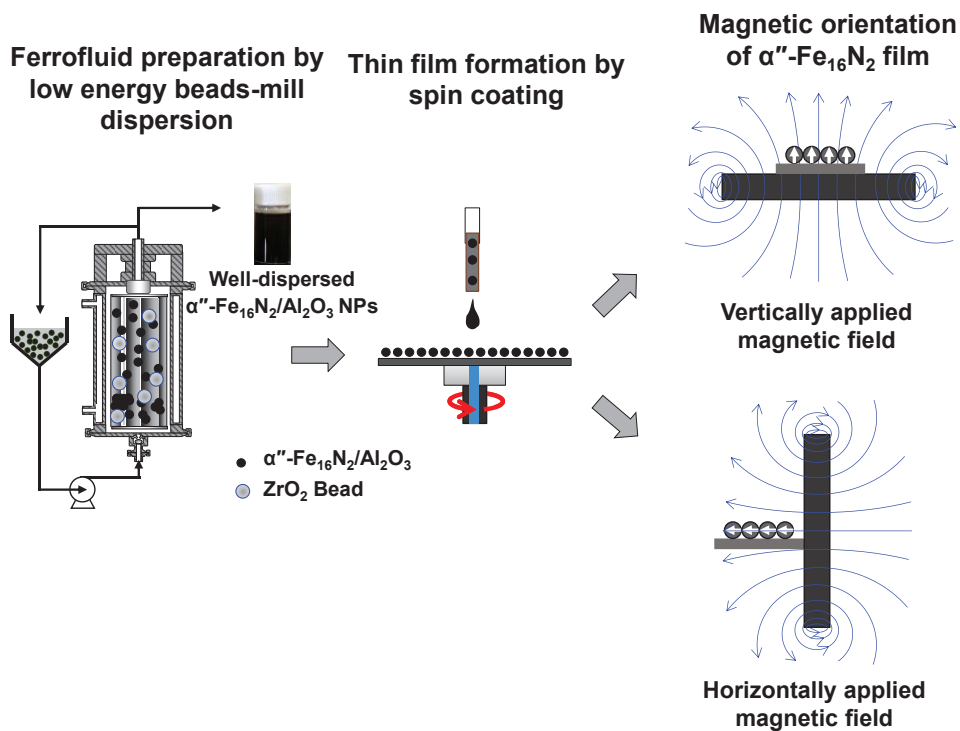


Figure 3.1. Schematic diagram of preparation of magnetically aligned α'' - $\text{Fe}_{16}\text{N}_2/\text{Al}_2\text{O}_3$ NPs film.

Table 3.1. Applied magnetic fields used in preparing various samples

Sample	Applied magnetic field	
	Magnetic field, H (T)	Direction
V0	0	-
V1	0.6	vertical
V2	0.9	vertical
V3	1.2	Vertical
H	0.6	Horizontal
R	0 (powder)	-

3.2.3 Characterization

The morphologies of the prepared α'' -Fe₁₆N₂/Al₂O₃ NP films were observed using field-emission scanning electron microscopy (FE SEM; Hitachi S-5000, Japan) and transmission electron microscopy (TEM; JEM-300F, JEOL Co., Ltd, Japan). The crystalline structures of the films were examined using X-ray diffraction (XRD; D2 Phaser, Bruker, Germany). The magnetic properties were evaluated using a superconducting quantum interference device (SQUID; Quantum Design, USA). Magnetization was measured as a function of the applied field from 1 to 50 kOe at 300 K.

3.3 Results and discussion

Figure 3.2 shows SEM (a) and TEM (b) images of core-shell single-domain α'' -Fe₁₆N₂/Al₂O₃ NPs. The SEM image shows the as-prepared NPs, and the TEM image shows the NPs after bead-mill dispersion. The inset figure shows the cross-sectional TEM image after bead-mill dispersion. The particles are single-domain NPs of an average size of approximately 50 nm, with a shell thickness of 4 nm. Because the α'' -Fe₁₆N₂/Al₂O₃ NPs were prepared by the gas phase method at high temperature, it is very difficult to obtain monodisperse NPs. The NP samples were similar to those described in our recent study [20].

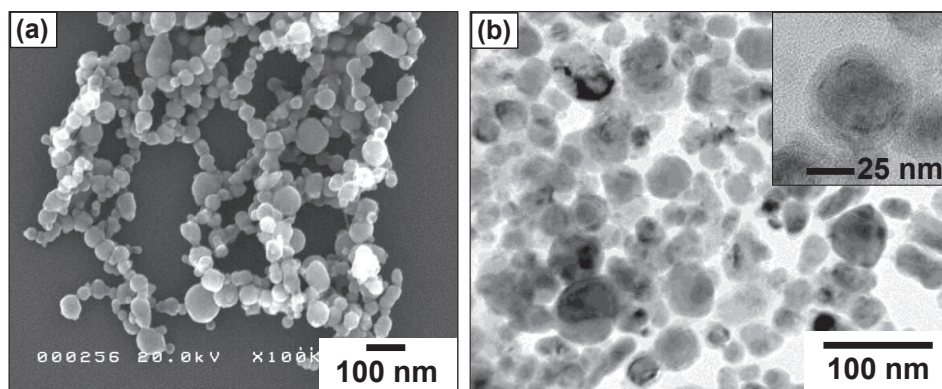


Figure 3.2. SEM (a) and TEM (b) images of α'' -Fe₁₆N₂/Al₂O₃ NPs; inset shows cross-sectional TEM image.

Figure 3.3 (a) shows a SEM image of the surface of the spin-coated α'' -Fe₁₆N₂/Al₂O₃ NP film under a vertically applied magnetic field, viewed at a tilt angle of 40°. The film surface is wavy because of the thickness of the resin. The film surface was covered with resin to maintain the NP arrangement in the film, as shown in **Figure 3.3** (b), which shows a cross-section of a densely packed core-shell α'' -Fe₁₆N₂/Al₂O₃ NP film of thickness \sim 1 μ m. The dense packing of

the α'' -Fe₁₆N₂/Al₂O₃ NPs in the film is clearly observed. This packing results from the well-dispersed state of the spherical NPs.

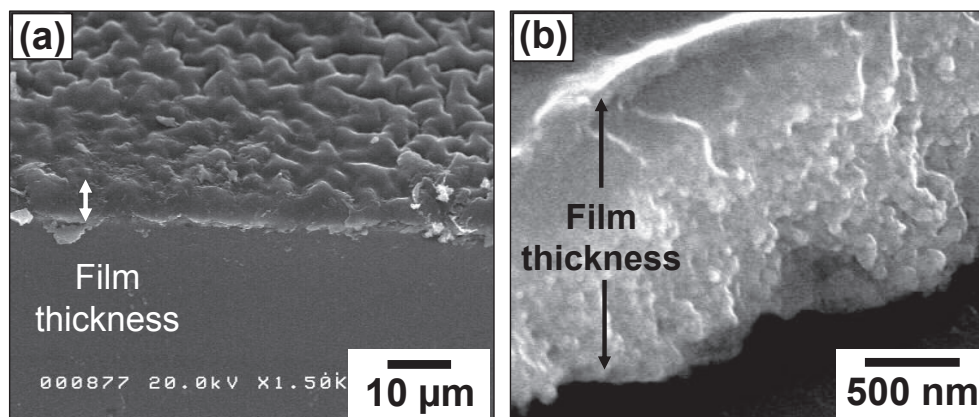


Figure 3.3. SEM images of surface and cross-section of spin-coated α'' -Fe₁₆N₂/Al₂O₃ NP film under vertical magnetic field, viewed at a tilt angle of 40°: low (a) and high (b) magnification.

The alignment of the α'' -Fe₁₆N₂ NPs can be carried out using two strategies, i.e., aligning the magnetic moment and aligning the easy c-axis of the particle. Aligning the easy c-axis, simply called the c-axis, of the particle is preferable due to the lower energy required. However, this strategy is applicable for only well-dispersed particles, where each of the particles can move freely. In the case of agglomerated particles, the alignment of the NPs can be performed only by the first strategy. Consequently, alignment of the magnetic moment in agglomerated particles requires high energy. XRD was used to determine the alignment of the c-axis of the α'' -Fe₁₆N₂ NP crystal inside the film. Due to the rotation of the particle (Brownian rotation) during the alignment process, the c-axis and the magnetic moment of the particles were aligned in the same direction along the magnetic field. In other words, the alignment of the c-axis represents the alignment of the magnetic moment. **Figure 3.4** shows typical XRD patterns of core-shell α'' -Fe₁₆N₂/Al₂O₃ NP powder and films; the vertical magnetic fields applied to the films varied from 0 to 1.2 T. A comparison of the XRD pattern of the α'' -Fe₁₆N₂/Al₂O₃ NP film without an applied magnetic field (sample V0) with that of the powder (R) shows that the (103), (213), (004), and (224) diffraction peaks of α'' -Fe₁₆N₂ disappeared in the film. For the films with higher vertically applied magnetic fields (samples V1, V2, and V3), (004) and (224) diffraction peaks of α'' -Fe₁₆N₂ appeared, and their intensities increased with the increasing magnetic field strength, whereas the (220) intensity decreased significantly, as shown in **Figure 3.4**.

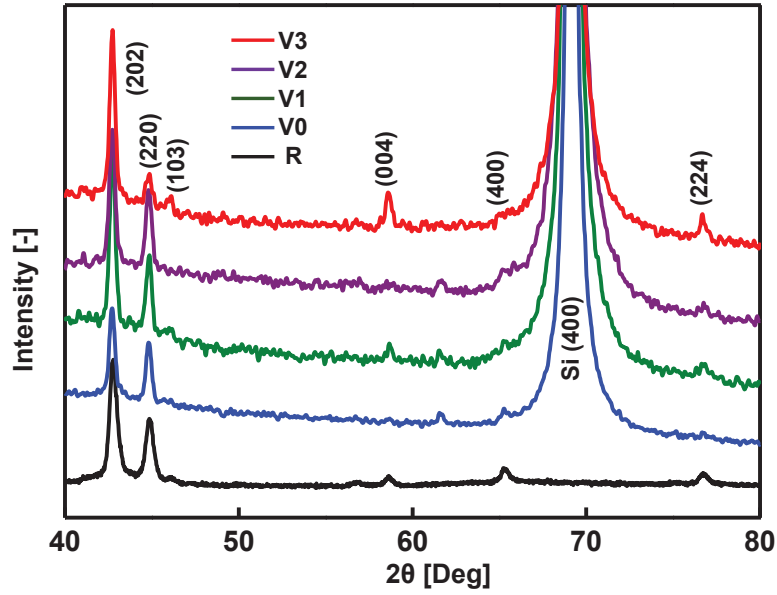


Figure 3.4. XRD patterns of α'' -Fe₁₆N₂/Al₂O₃ NPs and films under various applied magnetic fields.

The (004) peak has a vertical direction along the c-axis direction. If the (004) peak increased, it means that more of the c-axes of the particles are aligned in the vertical direction. From **Figure 3.4**, the intensity of the (004) diffraction peak of samples V1, V2, and V3 increased, which shows the vertical alignment of the NPs. However, the horizontal direction was shown by the (220) peak. This explains why the (220) peak decreased upon increasing the applied magnetic field strength, which means that the vertically aligned c-axis increased. However, the presence of (103) and (224) peaks shows that not all the c-axes are aligned perfectly in the vertical direction. The disappearance of the (400) peak in the pattern of the vertically aligned film suggests that no c-axes are aligned in the horizontal direction. The degree of alignment of the magnetic moment or c-axis, which is generally represented by the Lotgering factor (LF), can be calculated from the intensities of the XRD peaks, obtained in the conventional $2\theta/\theta$ scanning mode, using the following equation [21]:

$$LF = \frac{p - p_0}{1 - p_0} \quad (3.1)$$

where p is the ratio of the summation of the peak intensities corresponding to the preferred alignment axis to the summation of all the diffraction peaks in particle-aligned materials; p_0 is the p of a material with a random particle distribution.

The LF values were calculated using the above equation from the intensities of the (004) and (224) peaks because those peaks have a vertical direction. Therefore, the degree of c-axis

alignment can be evaluated from the enhancement of their intensity upon increasing the vertical magnetic field strength.

The LF values of the vertically aligned c-axis increased to 35% when the magnetic field was increased to 1.2 T (V3), as shown in **Table 3.2**. These results show that 35% of the α'' -Fe₁₆N₂ NPs in the film were vertically aligned; therefore, a stronger magnetic field is necessary to increase the alignment of the c-axis of the NPs in the film. It was estimated that an 11 T magnetic field would be needed to perfectly align (LF = 100%) the c-axis in the vertical direction. Contrary to the case where a magnetic field was applied during the synthesis of NPs, the application of a magnetic field during film preparation did not affect the morphology, crystal structure, or magnetic domain structure of the α'' -Fe₁₆N₂/Al₂O₃ NPs [22-26]. Instead, it only aligned the magnetic moment and c-axis of the NPs along the magnetic field direction.

Table 3.2. Orientations of vertically aligned α'' -Fe₁₆N₂ NP films

Sample	Alignment [LF (%)]
R	0
V0	28
V1	33
V2	33
V3	35

An LF value of 28% was obtained for the film prepared without a magnetic field (sample V0), showing that the alignment of the magnetic moment of the NPs occurred even when no magnetic field was applied. This alignment may arise from magnetic interactions between NPs, forming a chain with a head-to-tail arrangement of magnetic dipole moments [12, 27]. This alignment was parallel to the Si wafer due to surface interactions between the NPs and the Si wafer. The SEM image in **Figure 3.2** confirms that the α'' -Fe₁₆N₂ NPs form a chain as a result of the magnetic interactions between particles. The LF values of all the samples and their directions are summarized in **Table 3.2**.

Figure 3.5 shows the magnetic hysteresis loops of the randomly and vertically aligned films obtained by SQUID measurements at 300 K; these have been corrected by the effect of demagnetization. For each M–H loop, the magnetization is normalized by the saturation magnetization (M_s) of the film. The shape of the hysteresis loops approaches rectangular with the increase in the applied magnetic field, as clearly shown in the figure. A complete alignment of the c-axis of the NPs should ideally result in a rectangular hysteresis loop with a magnetic remanence ratio (M_r/M_s) = 1. The M_s values of the films were ~409 emu per cc or 124.54 emu

per gr film, and the Hc and Mr values of the vertically aligned film increased by 24% and 66%, respectively, upon increasing the applied magnetic field to 1.2 T. This increase in Hc and Mr is strongly related to the c-axis rotation phenomenon.

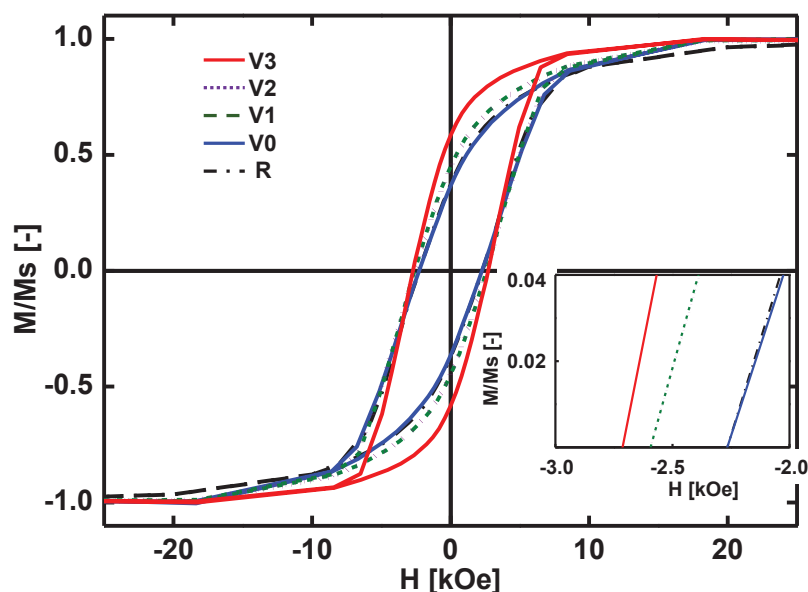


Figure 3.5. Hysteresis loops of α'' -Fe₁₆N₂/Al₂O₃ NPs and films under various applied magnetic fields; inset shows changes in coercivity (Hc).

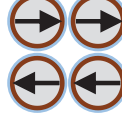
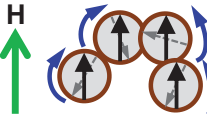
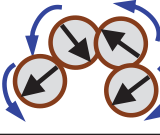
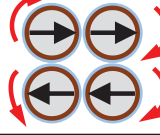
The c-axis rotation phenomenon was different for well-dispersed and aggregated NPs. The differences in the alignment phenomena of the magnetic moment upon applying a magnetic field between well-dispersed and agglomerated NPs are illustrated in Table 3.3.

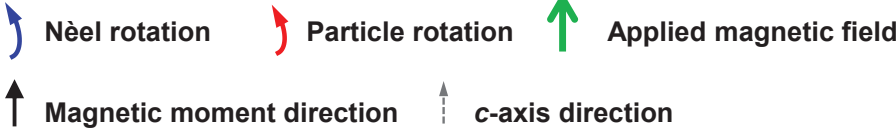
In the case of well-dispersed NPs, the particles are able to move freely, forming magnetic dipole coupling among NPs. By applying a magnetic field, the c-axis of the particle will be easily aligned, where in the case of single domain α'' -Fe₁₆N₂ NPs, the alignment of the c-axis means the alignment of its magnetic moment. This means that the magnetic moment and c-axis have the same direction. However, if the NPs were agglomerated, a higher energy is required to align the magnetic moment of the NPs because the particle cannot move freely. In other words, only Néel rotation will occur instead of particle rotation. This means that the magnetic moment and the c-axis have different directions.

By aligning the magnetic moment of the well-dispersed α'' -Fe₁₆N₂ NPs under a magnetic field and then fixing it using resin, the magnetic moment and the c-axis will be aligned in the same direction, along the magnetic field. This alignment of the magnetic moment results in an increase in the magnetic remanence of the film, as shown in the illustration in Table 3.3. The alignment of the magnetic moment of the particles influences the rotation of the magnetic moment during SQUID measurement, resulting in a different hysteresis curve. Applying a

magnetic field results in an improvement of the magnetic performance of the film, i.e., magnetic remanence (M_r) and coercivity (H_c).

Table 3.3. Illustration of alignment phenomena of magnetic moment in the agglomerated and well-dispersed magnetic NPs

Condition	Agglomerated NPs	Dispersed NPs	Fixed Dispersed NPs under magnetic field
As prepared			
Under magnetic field M_s			
Removal of magnetic field M_r			



The increase in both the H_c and M_r/M_s values with the c-axis alignment was also observed on SmCO_5 NPs, where a strong magnetic interaction occurred among isolated nanoparticles [10]. The magnetic properties of the agglomerated $\alpha''\text{-Fe}_{16}\text{N}_2$ films were higher than those of the well-dispersed film, likely due to the effects of the resin present in the film, which is a nonmagnetic material [28-30].

Significantly higher energy products $[(BH)_{\max}]$ were also obtained for the $\alpha''\text{-Fe}_{16}\text{N}_2$ films under a magnetic field than for that without a magnetic field; for example, $(BH)_{\max}$ value up to 1.211 MGOe was obtained for the film prepared using a magnetic field of 1.2 T, compared with a $(BH)_{\max}$ value of 0.465 MGOe for the film prepared without a magnetic field. These $(BH)_{\max}$ values are considerably lower than that of the $\alpha''\text{-Fe}_{16}\text{N}_2$ NPs, which is 2.029 MGOe. This increase in the maximum energy product occurs because the film consists of well-dispersed NPs; as we previously reported [19], the H_c value of well-dispersed $\alpha''\text{-Fe}_{16}\text{N}_2$ NPs is smaller than that of agglomerated particles because of the strong exchange interactions among the particles [31]. The $(BH)_{\max}$ for an applied magnetic field of 0.9 T was slightly lower, possibly because of the deviation in the estimation of the film volume. Because $(BH)_{\max}$

strongly depends on the magnetic coercivity, the application of a stronger magnetic field, which increases the coercivity, also increases $(BH)_{\max}$. The effect of the magnetic field strength on these magnetic properties of α'' -Fe₁₆N₂ films are shown in **Figure 3.6**. These results confirm that the alignment of the magnetic moment of the particles in the film significantly enhances its magnetic performance. Application of a magnetic field during the synthesis of the magnetic NPs also enhanced the magnetic properties of the prepared NPs [32].

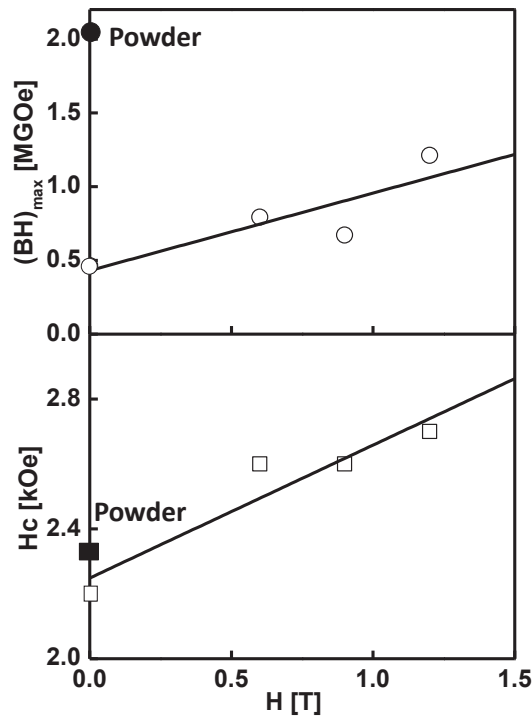


Figure 3.6. Maximum energy product and magnetic coercivity of the α'' -Fe₁₆N₂/Al₂O₃ NP film as a function of the applied magnetic field.

For comparison, we synthesized an α'' -Fe₁₆N₂/Al₂O₃ magnetic film under a horizontal magnetic field of 0.6 T. **Figure 3.7** (a) and b show the XRD patterns and hysteresis loops, respectively, of the horizontally aligned (sample H) α'' -Fe₁₆N₂/Al₂O₃ film and the film prepared without a magnetic field (sample V0). For the horizontally aligned film, (224) and (400) α'' -Fe₁₆N₂ diffraction peaks were observed, and the intensity of the (220) peak was higher than that for randomly aligned and vertically aligned films, which are shown in **Figure 3.4**. The appearance of a (400) peak for the horizontally aligned film suggests that there are c-axes of the particles aligned in the horizontal direction. The horizontally aligned film shows a higher-intensity (220) peak, indicating that many c-axes are aligned in the horizontal direction.

For comparison with the vertically aligned film, the degree of alignment of the magnetic moment, LF, of the horizontally aligned film was evaluated from the intensities of the (004)

and (224) diffraction peaks. The LF value was 27%. The smaller LF value than those for the randomly and vertically aligned films confirms that the c-axis of the particles was aligned in the horizontal direction. This value of LF is in the vertical direction, meaning that the NPs were 73% horizontally aligned. The XRD pattern of sample H shows that the intensity ratio of the (202) and (220) α'' -Fe₁₆N₂ NPs diffraction peaks was similar to that of sample V0 (without a magnetic field), which is shown in **Figure 3.4**. This indicates that the c-axes of the NPs in the film prepared without a magnetic field were aligned in the horizontal direction.

The magnetic properties of the horizontally aligned film (sample H) are shown by the demagnetization field corrected hysteresis loop in **Figure 3.7 (b)**. The application of a magnetic field of 0.6 T in the horizontal direction impairs the magnetic properties [M_r/M_s , H_c , and $(BH)_{max}$ values of 0.32, 2.1 kOe, and 0.42 MG Oe, respectively] compared with those of the film sample prepared without a magnetic field (sample V0). These results show that the magnetic properties of the α'' -Fe₁₆N₂ magnetic film are governed by the alignment of the magnetic moment of the NPs, which can be tuned by applying an external magnetic field during film preparation.

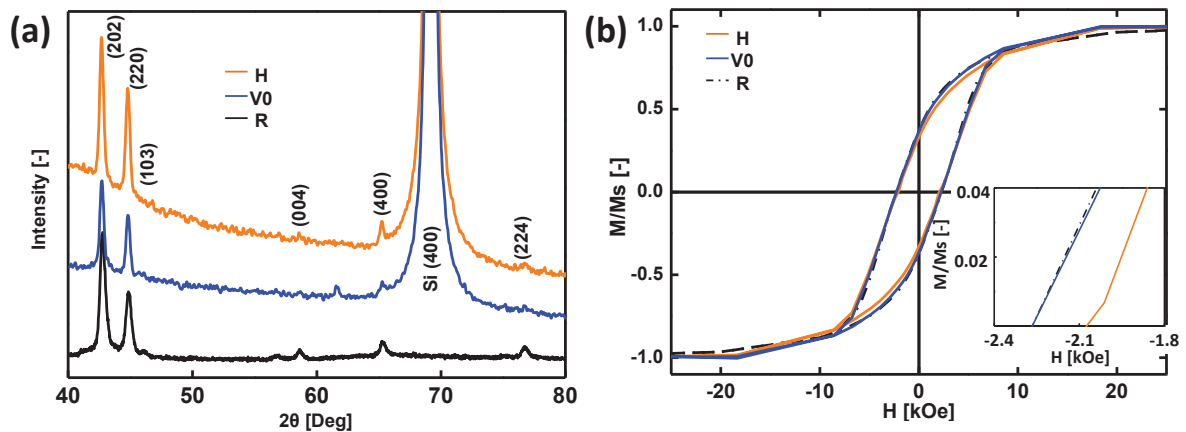


Figure 3.7. XRD pattern (a) and magnetic hysteresis loop (b) of α'' -Fe₁₆N₂/Al₂O₃ NP film under a horizontally applied magnetic field.

The relationship between the alignment of the magnetic moment of the α'' -Fe₁₆N₂ NPs and the magnetic performance of the film, as shown in **Figure 3.8**, confirms that both H_c and $(BH)_{max}$ increased with increasing the alignment of the magnetic moment. It was estimated that the maximum H_c and $(BH)_{max}$ values were approximately 8 kOe and 7 MGOe, respectively, at the perfect alignment. The low value of $(BH)_{max}$ value may arise from the presence of resin in the film. These results are important for the development of spintronic device applications and

also suggest the possibility of the nanostructuring of bulk anisotropic magnetic materials by magnetic field induced compaction of single-domain α'' -Fe₁₆N₂ NPs.

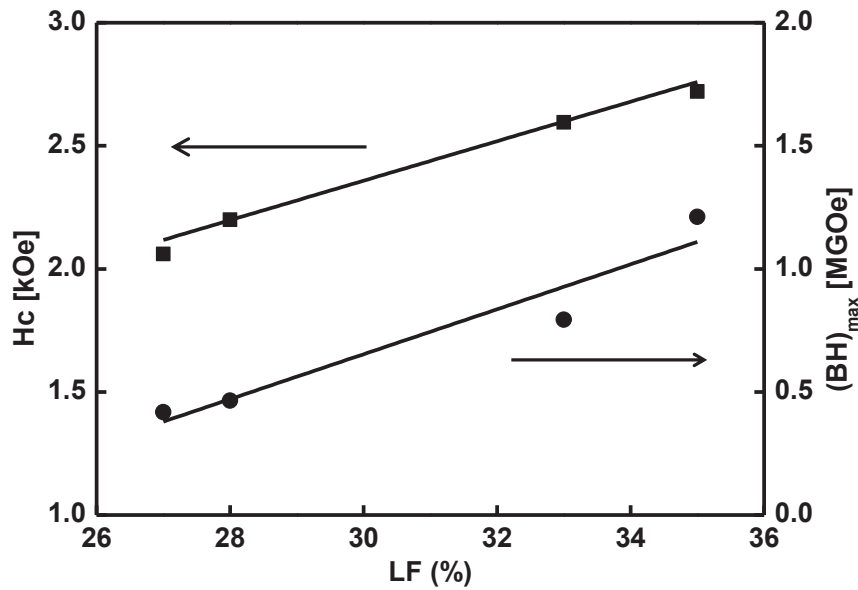


Figure 3.8. Relationship of magnetic NP alignment with magnetic properties of α'' -Fe₁₆N₂ NP film.

3. 4 Conclusion

The magnetic field induced single domain core-shell α'' -Fe₁₆N₂ NP films show densely packed NP assemblies. The XRD and SQUID analyses show increases in the alignment of the magnetic moment of the NPs and the magnetic properties with the increase in the magnetic field applied vertically to the film substrate. At 1.2 T, the alignment of the magnetic moment increased by 35%, whereas the Hc, Mr, and (BH)_{max} increased by 24%, 66%, and 160%, respectively. The maximum Hc and (BH)_{max} values can be estimated from the relationship between the alignment of the magnetic moment and the magnetic properties to be approximately 8 kOe and 7 MGoe, respectively. These results imply that core-shell α'' -Fe₁₆N₂/Al₂O₃ NPs have the potential for the construction of bulk magnetic materials with tunable magnetic performances by applying a magnetic field.

3.5 References

- [1] Sun S 2006 Recent advances in chemical synthesis, self-assembly, and applications of FePt nanoparticles *Adv. Mater.* **18** 393-403

- [2] Zulhijah R, Yoshimi K, Nandiyanto ABD, Ogi T, Iwaki T, Nakamura K, Okuyama K 2014 α'' -Fe₁₆N₂ phase formation of plasma-synthesized core-shell type α -Fe nanoparticles under various conditions *Adv. Powder Technol.* **25** 582-90
- [3] Akdogan O, Li W, Balasubramanian B, Sellmyer DJ, Hadjipanayis GC 2013 Effect of exchange interactions on the coercivity of SmCo₅ nanoparticles made by cluster beam deposition *Adv. Funct. Mater.* **23** 3262-7
- [4] Poudyal N, Liu JP 2013 Advances in nanostructured permanent magnets research *J. Phys. D: Appl. Phys.* **46** 043001
- [5] Chappert C, Fert A, Van Dau FN 2007 The emergence of spin electronics in data storage *Nature Materials* **6** 813 - 23
- [6] Sellmyer DJ 2002 Applied physics: Strong magnets by self-assembly *Nature* **420** 374-5
- [7] Balamurugan B, Das B, Mukherjee P, Sellmyer DJ 2014 Development of nanoparticle-based permanent-magnet materials challenges and advances *REPM* 429-3
- [8] Issa B, Obaidat IM, Albiss BA, Haik Y 2013 Magnetic nanoparticles: Surface effects and properties related to biomedicine applications *Int. J. Mol. Sci.* **14** 21266-305
- [9] Frey NA, Peng S, Cheng K, Sun S 2009 Magnetic nanoparticles: synthesis, functionalization, and applications in bioimaging and magnetic energy storage *Chem. Soc. Rev.* **38** 2532-42
- [10] Balamurugan B, Sellmyer DJ, Hadjipanayis GC, Skomski R 2012 Prospects for nanoparticle-based permanent magnets *Scripta Mater.* **67** 542-7
- [11] Black CT, Murray CB, Sandstrom RL, Sun S 2000 Spin-dependent tunneling in self-assembled cobalt-nanocrystal superlattices *Science* **290** 1131-4
- [12] Singamaneni S, Bliznyuk VN, Binek C, Tsymbal EY 2011 Magnetic nanoparticles: Recent advances in synthesis, self-assembly and applications *J. Mater. Chem.* **21** 16819
- [13] Fried T, Shemer G, Markovich G 2001 Ordered two-dimensional arrays of ferrite nanoparticles *Adv. Mater.* **13** 1158-61
- [14] Ogi T, Nandiyanto ABD, Kusakibaru Y, Iwaki T, Nakamura K, Okuyama K 2013 Facile synthesis of single-phase spherical α'' -Fe₁₆N₂/Al₂O₃ core-shell nanoparticles via a gas-phase method *J. Appl. Phys.* **113** 164301
- [15] Zulhijah R, Nandiyanto ABD, Ogi T, Iwaki T, Nakamura K, Okuyama K 2014 Gas phase preparation of spherical core-shell α'' -Fe₁₆N₂/SiO₂ magnetic nanoparticles *Nanoscale* **6** 6487-91

- [16] Zulhijah R, Nandiyanto ABD, Ogi T, Iwaki T, Nakamura K, Okuyama K 2015 Effect of oxidation on α "-Fe₁₆N₂ phase formation from plasma-synthesized spherical core-shell α -Fe/Al₂O₃ nanoparticles *J. Magn. Magn. Mater.* **381** 89-98
- [17] Bhattacharyya S 2015 Iron nitride family at reduced dimensions: A review of their synthesis protocols and structural and magnetic properties *J. Phys. Chem. C* **119** 1601-22
- [18] Dugay J, Tan RP, Loubat A, Lacroix LM, Carrey J, Fazzini PF, Blon T, Mayoral A, Chaudret B, Respaud M 2014 Tuning deposition of magnetic metallic nanoparticles from periodic pattern to thin film entrainment by dip coating method *Langmuir* **30** 9028-35
- [19] Zulhijah R, Suhendi A, Yoshimi K, Kartikowati CW, Ogi T, Iwaki T, Okuyama K 2015 Low-energy bead-mill dispersion of agglomerated core-shell α -Fe/Al₂O₃ and α "-Fe₁₆N₂/Al₂O₃ ferromagnetic nanoparticles in toluene *Langmuir* **31** 6011-9
- [20] Suhendi A, Kartikowati CW, Zulhijah R, Ogi T, Iwaki T, Okuyama K 2015 Preparation and characterization of magnetic films of well-dispersed single domain of core-shell α "-Fe₁₆N₂/Al₂O₃ nanoparticles *Adv. Powder Technol.* **26** 1618-23
- [21] Furushima R, Tanaka S, Kato Z, Uematsu K 2010 Orientation distribution–Lotgering factor relationship in a polycrystalline material—as an example of bismuth titanate prepared by a magnetic field *J. Ceram. Soc. Jpn.* **118** 921-6
- [22] Wang J, Chen Q, Zeng C, Hou B 2004 Magnetic-field-induced growth of single-crystalline Fe₃O₄ nanowires *Adv. Mater.* **16** 137–40
- [23] Wang J, Chen Q, Li X, Shi L, Peng Z, Zeng C 2004 Disappearing of the Verwey transition in magnetite nanoparticles synthesized under a magnetic field: implications for the origin of charge ordering *Chem. Phys. Lett.* **390** 55-8
- [24] Su Y, Zhang Y, Wei H, Zhang L, Zhao J, Yang Z, Zhang Y 2012 Magnetic-field-induced diameter-selective synthesis of single-walled carbon nanotubes *Nanoscale* **4** 1717-21
- [25] Keidar M, Levchenko I, Arbel T, Alexander M, Waas AM, Ostrikov K 2008 Increasing the length of single-wall carbon nanotubes in a magnetically enhanced arc discharge *Appl. Phys. Lett.* **92** 043129
- [26] Su Y, Zhang Y, Wei H, Yang Z, Kong ESW, Zhang Y 2012 Diameter-control of single-walled carbon nanotubes produced by magnetic field-assisted arc discharge *Carbon* **50** 2556-62

- [27] Morup S, Hansen MF, Frandsen C 2010 Magnetic interactions between nanoparticles *Beilstein J. Nanotechnol.* **1** 182-90
- [28] Kim TK, Takahashi M 1972 New magnetic material having ultrahigh magnetic moment *Appl. Phys. Lett.* **20** 492-4
- [29] Sugita Y, Takahashi H, Komuro M, Igarashi M, Imura R, Kambe T 1996 Magnetic and electrical properties of single-phase, single-crystal Fe₁₆N₂ films epitaxially grown by molecular beam epitaxy *J. Appl. Phys.* **79** 5576
- [30] Takahashi M, Shoji H, Takahashi H, Wakiyama T, Kinoshita M, Ohta W 1993 Synthesis of Fe₁₆N₂ films by using reactive plasma *IEEE Trans. Magn.* **29** 3040 - 5
- [31] Kechrakos D, Trohidou KN 2003 Competition between dipolar and exchange interparticle interactions in magnetic nanoparticle films *J. Magn. Magn. Mater.* **262** 107-10
- [32] Hu L, Zhang R, Chen Q 2014 Synthesis and assembly of nanomaterials under magnetic fields *Nanoscale* **6** 14064-105

Chapter 4

Synthesis of α'' -Fe₁₆N₂/Polyvinylpyrrolidone magnetic nanocomposite fibers under magnetic field

4.1 Introduction

Nanocomposite fibers with magnetic nanoparticles (NPs) embedded in the polymer matrix are increasingly gaining attention due to the fact that the geometrical dimensions of these materials are comparable to key magnetic length scales, such as the exchange length or the domain wall width [1, 2]. These materials also have potential applications in many fields, such as magnetic sensors, magnetic filters, microwave absorbers, tissue-engineering scaffolds, electromagnetic wave absorbers, magnetic catalysts, ferroelectric photovoltaic devices, and magnetic hyperthermia [3-6]. Among the methods used to synthesize polymeric fibers, electrospinning is a versatile and effective technique for producing fibers with diameters ranging from a few hundred nanometres to several micrometres [7]. The relatively high production rate and simplicity of the setup make electrospinning highly attractive to both academia and industry.

Several studies of the synthesis of magnetic polymeric fibers containing magnetic NPs, i.e. γ -Fe₃O₄ NPs, via magnetic-field assisted electrospinning have been reported [8-10]. Yang et al fabricated well-aligned poly(vinyl alcohol) fibers by placing two magnets at the sides of the collector during electrospinning [8]. Wang et al used a similar magnetic-field configuration to produce aligned polyvinylpyrrolidone (PVP)/Fe₃O₄ fibers, but further plasma treatments were conducted to obtain pure Fe₃O₄ fibers with an average diameter of 200 nm. A different configuration was reported by Ajao et al in which a cylindrical magnet was employed to produce well-aligned poly(ethylene oxide) [10]. However, the effects of the applied magnetic field on the fiber diameter and magnetic properties have not been thoroughly analyzed, despite the production of well-aligned fibers.

The magnetic performances of magnetic nanocomposite fibers are significantly affected by the magnetic properties of the embedded NPs. It has been reported that α'' -Fe₁₆N₂ NPs have the highest saturation magnetization and a high magnetic moment, and have potential as rare-earth-free magnetic materials [11]. Recently, our group successfully synthesized core-shell structured α'' -Fe₁₆N₂ NPs from α -Fe and Al₂O₃ as the core and shell, respectively, via a gas-phase method [12-14]. The obtained core-shell magnetic NPs consisted of partially

agglomerated and aggregated α'' -Fe₁₆N₂ NPs, thus dispersion is necessary to prepare well-dispersed single-domain α'' -Fe₁₆N₂ NPs. In our recent research, we have succeeded in dispersing these core-shell α'' -Fe₁₆N₂ NPs into primary particle size in the organic solvent without destroying their structure via low-energy bead-mill dispersion [15]. Single-domain MNPs are of tremendous interest both from a fundamental viewpoint and for their potential applications due to their unique magnetic properties, such as enhanced coercivity, and chemical catalytic properties, integrated with their high specific surface area [16].

Based on these results, we found that these NPs, with their excellent magnetic properties, have a potential use in highly magnetic nanocomposite fibers. Further, to the best of our knowledge, there is no report of the use of core-shell α'' -Fe₁₆N₂ NPs in nanocomposite fibers. Therefore, the synthesis of high-magnetic-performance fibers using α'' -Fe₁₆N₂ NPs would be an interesting advance in the development of magnetic nanocomposite fibers.

In this research, the synthesis of magnetic nanocomposite fibers containing core-shell α'' -Fe₁₆N₂/Al₂O₃ NPs in PVP via magneto-electrospinning was reported. A ferrofluid of dispersed α'' -Fe₁₆N₂ NPs in a PVP-toluene-methanol solution was used as the precursor solution. We compared magnetic fibers containing α'' -Fe₁₆N₂ NPs acting as a hard magnet with those containing a soft magnet, i.e. α -Fe NPs, to investigate the effects of NP magnetic strength on the fiber properties. Two different magnetic NP loadings were used to investigate their effect on the fiber formation. The effect of the applied magnetic field on the morphology and magnetic performance of electrospun magnetic nanocomposite fibers was examined by applying an external magnetic field in the same direction as the electrospinning, which is expected to significantly improve the magnetic performance.

4. 2 Experimental

4.2.1 Preparation of raw materials

The core-shell single-domain α'' -Fe₁₆N₂/Al₂O₃ NPs used as the raw materials in this study were prepared via nitridation of core-shell single-domain α -Fe/Al₂O₃ NPs, which were synthesized and stored in a glove box with an N₂ environment, as reported in previous study [12]. The core-shell α -Fe/Al₂O₃ NPs were prepared using a one-step radio-frequency thermal plasma process [13]. The other raw materials, such as PVP (K-90), toluene (99.95%), and methanol (99.95%), were purchased from Kanto Chemicals, Tokyo, Japan, and were used without further treatment or purification.

4.2.2 Preparation of ferrofluid for electrospinning

Magnetic NP slurries were prepared from concentrated core-shell α'' -Fe₁₆N₂/Al₂O₃ and α -Fe/Al₂O₃ NPs dispersed in toluene. The NPs were obtained by a low-energy bead-mill dispersion process in same manner reported in our recent study [15]. The magnetic NP slurries were mixed with a PVP solution to make a ferrofluid precursor for electrospinning with two different loadings of 16.5 wt% and 28.4 wt% of magnetic NPs. The PVP solution was obtained by dissolving 15 wt% PVP in a mixture of toluene and methanol with a mass ratio of 1:1. The electrical conductivity of the ferrofluid precursors (WM-50EG, DKK-TOA Corp., Japan) is shown in **Table 4.1**. The electrical conductivity of the PVP solution was 129.9 $\mu\text{S m}^{-1}$.

Table 4.1. Electrical conductivities of ferrofluid precursors

Fibers	NPs loading	Electrical conductivity (mS/m)
α -Fe/PVP	28.4 wt%	0.434
	16.5 wt%	0.730
α'' -Fe ₁₆ N ₂ /PVP	28.4 wt%	0.483
	16.5 wt%	0.760

4.2.3 Magneto-electrospinning

An external magnetic field of 0.1 T was applied to the aluminum foil substrate perpendicular to the collector and parallel to the electric field in the electrospinning system, as shown in the schematic diagram of the magneto-electrospinning apparatus in **Figure 4.1**. The ferrofluids were loaded into a 1000 μl glass syringe with a stainless-steel needle and an inner diameter of 0.21 mm. The solution was fed through the needle using a syringe pump (PhD 2000, Harvard Apparatus) at a flow rate of 2–20 $\mu\text{l min}^{-1}$ to examine the effect of ferrofluid flow rate. The needle was connected to a high-voltage power supply (Matsusada HER 20R3, Matsusada Precision) with a dc voltage capacity of 20 kV. A positive electrical potential varying within a certain range was applied to the needle to create a stable Taylor cone. During the electrospinning process, the solvent evaporated and altered fibers were collected electrostatically on a grounded silicon wafer attached to the aluminum foil, which was placed 11 cm from the needle tip. The environment during electrospinning was kept at a temperature of (30 \pm 2) °C and a relative humidity of (30 \pm 5) %.

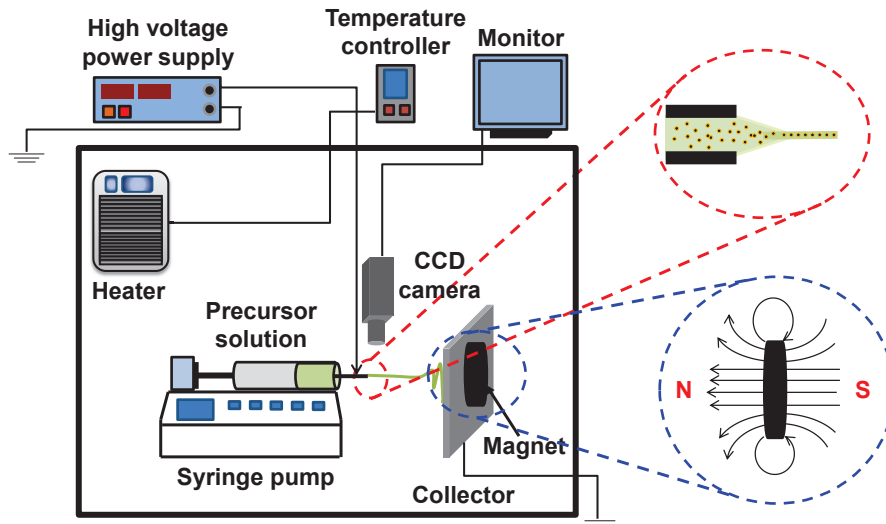


Figure 4.1. Schematic diagram of the magneto-electrospinning apparatus

4.2.4 Characterization

The morphologies of the prepared nanocomposite fibers were examined using field emission scanning electron microscopy (FE-SEM; Hitachi S-5000, Hitachi, Japan, operated at 20 kV) and transmission electron microscopy (TEM; JEM-3000F, JEOL Ltd, Japan). The fibers were also examined using x-ray diffraction (XRD; D2 Phaser, Bruker, Germany, Cu $K\alpha$ radiation, scanning range $2\theta=20^\circ\text{--}80^\circ$). A superconducting quantum interference device magnetometer (SQUID; MPMS 5XL, Quantum Design, Japan, operated at 300 K) was used to determine the magnetic properties of the prepared nanocomposite fibers.

4.3 Results and discussion

4.3.1 Core-shell $\alpha''\text{-Fe}_{16}\text{N}_2/\text{Al}_2\text{O}_3$ and $\alpha\text{-Fe}/\text{Al}_2\text{O}_3$ NPs

Figure 4.2 shows the morphologies of the core-shell $\alpha''\text{-Fe}_{16}\text{N}_2$ and $\alpha\text{-Fe}$ NPs. **Figure 4.2** (a), (d), (b), (e), and (c), (f) show the SEM and TEM images and size distributions, respectively, of the core-shell $\alpha''\text{-Fe}_{16}\text{N}_2$ and $\alpha\text{-Fe}$ NPs. The SEM images show the as-prepared magnetic NPs, and the TEM images show the NPs after bead-mill dispersion. The SEM images and particle size distributions show that before bead-mill dispersion, the $\alpha''\text{-Fe}_{16}\text{N}_2$ and $\alpha\text{-Fe}$ NPs both consisted of agglomerated spherical particles with average sizes of 48.4 and 46.9 nm, respectively. The TEM images confirmed that the $\alpha''\text{-Fe}_{16}\text{N}_2$ and $\alpha\text{-Fe}$ NPs were well dispersed after bead-mill dispersion. Furthermore, core-shell structures were observed for both types of NP with an average shell thickness of 4 nm.

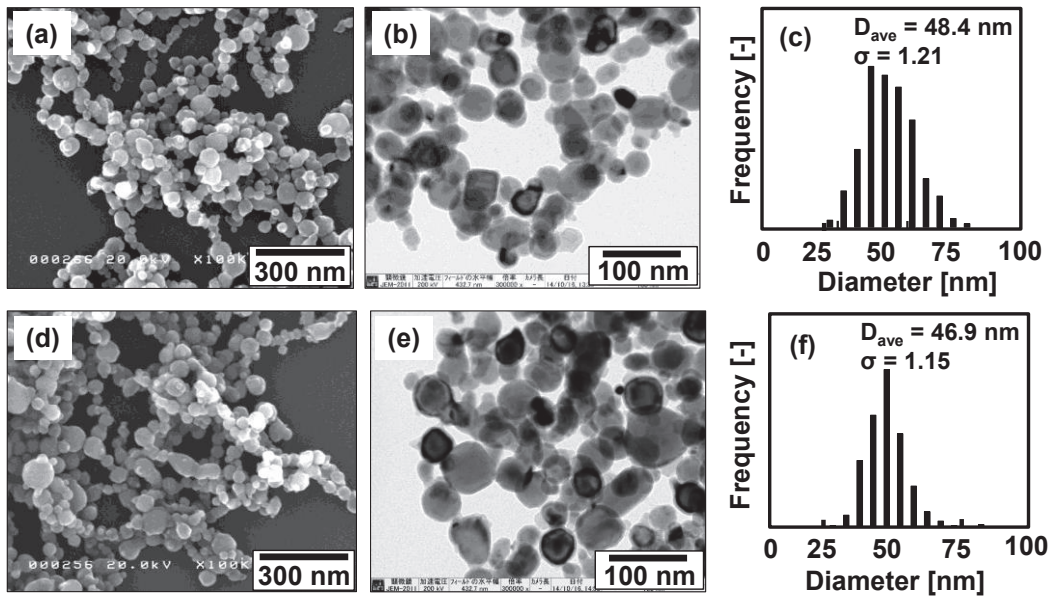


Figure 4.2 SEM and TEM images, and size distributions of core-shell α "- $Fe_{16}N_2/Al_2O_3$ (a), (b), (c) and α - Fe/Al_2O_3 (d), (e), (f) NPs, respectively.

4.3.2 Electrospun PVP fibers

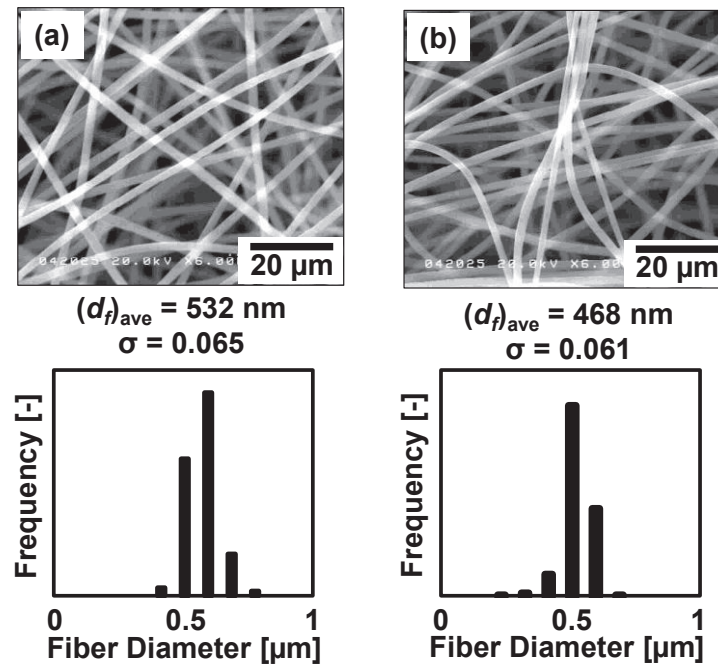


Figure 4.3 SEM images and size distributions of electrospun PVP fibers prepared without (a) and with (b) magnetic field.

The SEM images and size distributions of the electrospun PVP fibers without embedded magnetic NPs at fixed flow rate $2 \mu l \text{ min}^{-1}$ are shown in **Figure 4.3**. **Figure 4.3** (a) shows that the fibers prepared without the presence of a magnetic field have an average diameter of 532

nm, with a standard deviation of 0.065. After application of a magnetic field, as shown in **Figure 4.3** (b), the electrospun fiber's diameter became slightly smaller, with an average diameter of 468 nm and a standard deviation of 0.061. Application of a magnetic field increases the stability of the electrospinning jet, leading to the formation of fibers with smaller and more uniform diameter.

4.3.3 Electrospun magnetic nanocomposite fibers

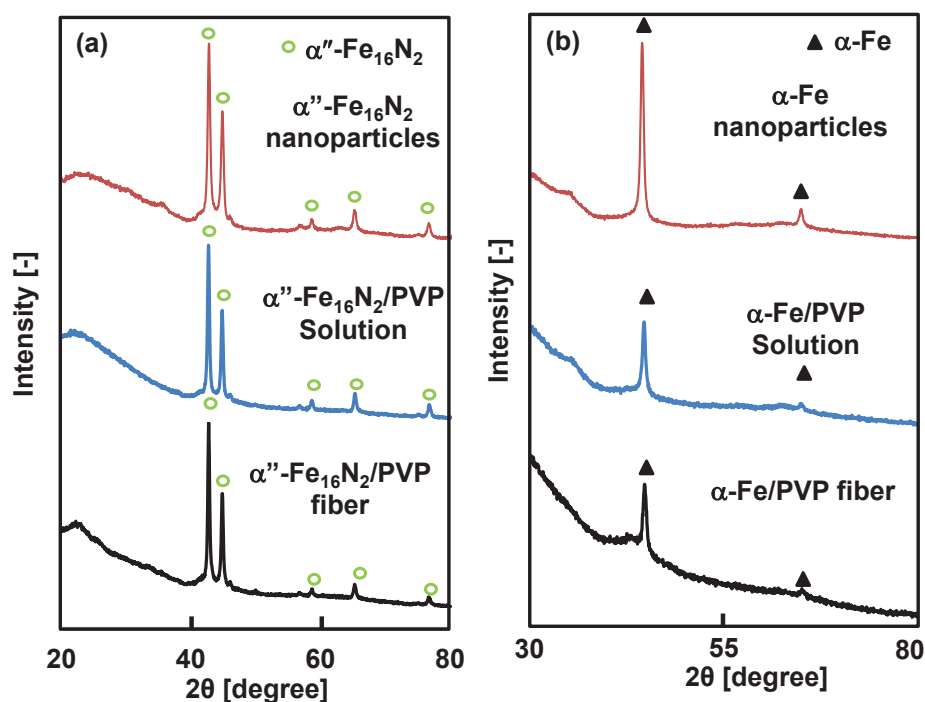


Figure 4.4. XRD patterns of the nanocomposite magnetic fibers with magnetic NP loadings of 28.4 wt%. (a) and (b) are α'' - Fe_{16}N_2 /PVP and α -Fe/PVP magnetic nanocomposite fibers, respectively.

The nanocomposite fiber was prepared by embedding magnetic NPs into the fibers. The XRD patterns of as-spun α'' - Fe_{16}N_2 and α -Fe magnetic nanocomposite fibers prepared with a magnetic field and magnetic NP loading of 28.4 wt% at fixed flow rate of $3 \mu\text{l min}^{-1}$ are shown in **Figure 4.4**. The plots show that there is no phase change observed in the XRD pattern of the well dispersed core-shell α'' - Fe_{16}N_2 and α -Fe NPs, solutions, and fibers. The crystal properties of the magnetic NPs after electrospinning are not significantly different from those of the particles before electrospinning. This indicates that there is no phase change of the magnetic NPs after the electrospinning process. A decrease in the peak intensities of both magnetic NPs

after electrospinning was observed, indicating the effect of the polymer used on the NPs in the nanocomposite fibers.

Figure 4.5 shows the TEM images of the as-spun magnetic α'' -Fe₁₆N₂ nanocomposite fibers with an NP loading of 28.4 wt% prepared without (a) and with (b) magnetic field. These images show that the core-shell α'' -Fe₁₆N₂ NPs are inside the fibers without any NPs on the fiber surface. The images show different NP distributions inside the fibers. For fibers prepared without the existence of magnetic field, the NPs are randomly distributed. However, after the applying the magnetic field, the NPs are aligned along the fiber and the diameter of the fiber is decreased. These results show that application of the magnetic field is not only reducing the fiber diameter but also aligning the NPs inside the fiber. This NPs alignment is possible because of the well-dispersed state of the NPs. **Figure 4.5** (c) and (d) show the SAED pattern and high-resolution TEM image of a α'' -Fe₁₆N₂ NP inside the fibers, respectively. These images confirm that the magnetic NP present was single-domain α'' -Fe₁₆N₂. The interplanar spacing is measured to be 5.47 Å, which is consistent with the (110) crystal structure of a bct α'' -Fe₁₆N₂ phase.

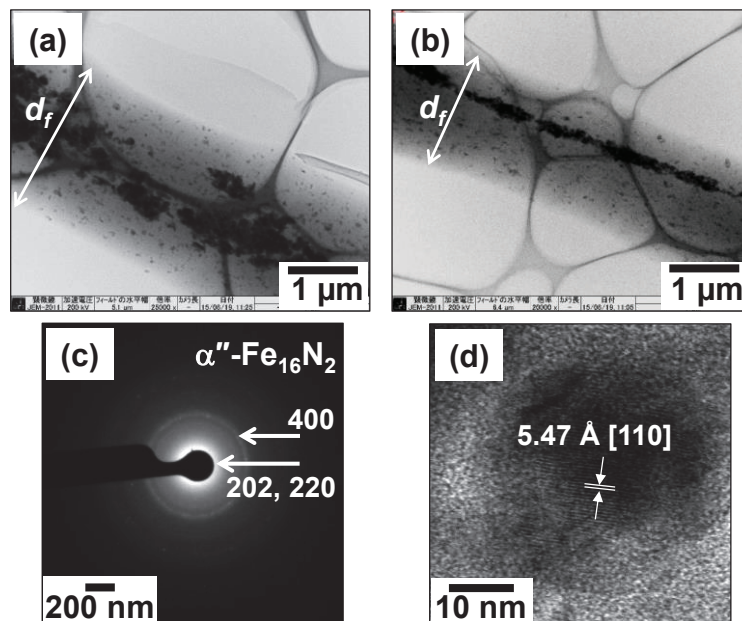


Figure 4.5. TEM images of magnetic α'' -Fe₁₆N₂/PVP nanocomposite fibers produced with an NP loading of 28.4 wt% without (a) and with (b) magnetic field. (c) and (d) are the SAED pattern and HRTEM image of α'' -Fe₁₆N₂ NP inside the fiber. White lines in panels (a) and (b) show the fiber diameter.

4.3.4 Evaluation of electrospun magnetic nanocomposite fibers

Table 4.2 shows the FE-SEM images of electrospun α'' -Fe₁₆N₂ and α -Fe magnetic nanocomposite fibers prepared without (a)–(d) and with (e)–(h) a magnetic field, at a fixed flow rate of 3 $\mu\text{l min}^{-1}$. The average diameters of the fibers prepared without a magnetic field shown in **Table 4.2** (a)–(d) are 1.84, 1.56, 2.35, and 1.69 μm , respectively. **Table 4.2** (e)–(h) shows the fibers prepared with a magnetic field, for which smaller average diameters of 1.25, 1.19, 1.44, and 1.09 μm were observed.

These findings confirm the results for electrospun PVP fibers, although the diameter of the composite fiber was larger than that of PVP alone. This increase was due to the addition of NPs inside the fibers. The fibers produced by electrospinning with a magnetic field applied also have more uniform diameter than those without the magnetic field. The details of the size distributions and standard deviations of the prepared fibers are given in **Table 4.3**. These results are in good agreement with previous reports that studied the effect of Fe₃O₄ NPs on magnetic-field-assisted electrospinning, although the magnetic field in these studies was applied perpendicular to the electric field. They explained that by applying a magnetic field during the electrospinning process, fibers with smaller and more uniform diameter were produced. However, the reason for the smaller diameter was not explained [17, 18].

The diameter of the α'' -Fe₁₆N₂ fibers was smaller than those of the α -Fe fibers. This is due to the electrical conductivity of the α -Fe solution, which is smaller than that of the α'' -Fe₁₆N₂ solution. The higher electrical conductivity produces a smaller jet diameter, which results in a smaller fiber diameter [19]. The electrical conductivity of the solution with a magnetic NP loading of 16.5 wt% was higher than that of the 28.4 wt% NP loading because the electrical conductivity of the solution of each precursor depends on the ratio of the toluene and methanol: the 16.5 wt% loading contained a larger amount of methanol. However, the diameters of the fibers with an NP loading of 28.4 wt% are smaller than those of 16.5 wt%. This is because the change of fiber diameter is not only influenced by electrical conductivity but also by the viscosity and magnetic NP content of the solutions. The solution with an NP loading of 28.4 wt% has a smaller viscosity and higher magnetic NP content than that with a loading of 16.5 wt%, leading to the formation of smaller diameter fibers.

Table 4.2. SEM images of magnetic α'' - Fe_{16}N_2 /PVP and α -Fe/PVP nanocomposite fibers at flow rate of 3 $\mu\text{l}/\text{min}$

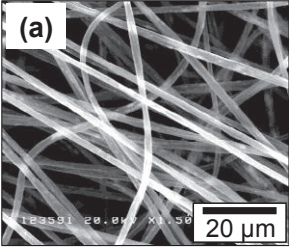
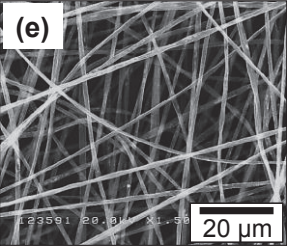
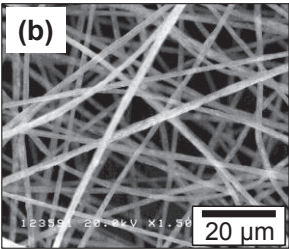
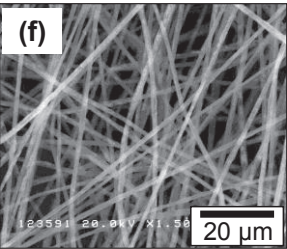
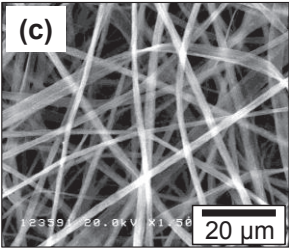
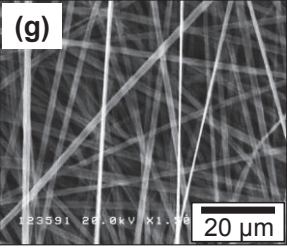
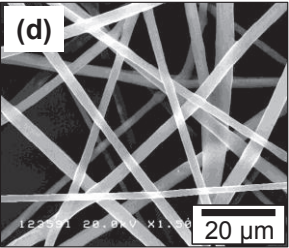
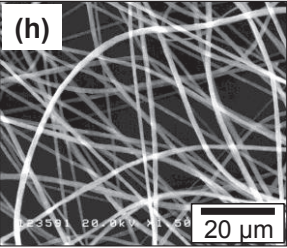
Fiber	MNPs content	Without magnetic field	With magnetic field
α'' - Fe_{16}N_2 /PVP	16.5 wt%		
	28.4 wt%		
α -Fe/PVP	16.5 wt%		
	28.4 wt%		

Table 4.3. Diameter distributions of nanocomposite fibers prepared without and with applied magnetic field.

Fiber	α'' -Fe ₁₆ N ₂ /PVP		α -Fe/PVP	
MNPs content	16.5 wt%	28.4 wt%	16.5 wt%	28.4 wt%
Without magnetic field				
With magnetic field				

4.3.4.1. Effect of flow rate on the fiber diameter

The fiber diameter is one of the most important physical properties of the electrospun fibers. Many researchers have developed analytical models of the relationship between the electrospinning parameters and fiber diameter. One of the most widely used models was reported by Fridrikh et al [20]. For a constant solution surface tension and permittivity, the equation can be simplified as follows:

$$d_f = \left[\frac{Q}{I} \right]^{\frac{2}{3}} \quad (4.1)$$

Here, d_f is the fiber diameter, Q is the flow rate, and I is the electric current. This model assumes that solvent evaporation is insignificant prior to attainment of the limiting diameter. Solvent evaporation changes the diameter but not the length of the fibers.

Figure 4.6 shows plots of the average diameter of α'' -Fe₁₆N₂ (a) and α -Fe (b) nanocomposite fibers against the inverse of the volume charge density Q/I for different MNP loadings on a log scale. The relationship between fiber diameter and flow rate obeys a power law for fibers prepared both without and with a magnetic field. Linear regression gives slopes, intercepts and R^2 values, which are summarized in **Table 4.4**. These results imply that the increase in the average diameter with increasing Q follows a power law, i.e. $d \approx (Q/I)^{0.612}$ and $d \approx (Q/I)^{0.427}$, for α'' -Fe₁₆N₂ fibers with an NP loading of 28.4 wt% prepared without and with a magnetic field, respectively. For α -Fe fibers, the power laws were $d \approx (Q/I)^{0.489}$ and $d \approx (Q/I)^{0.320}$.

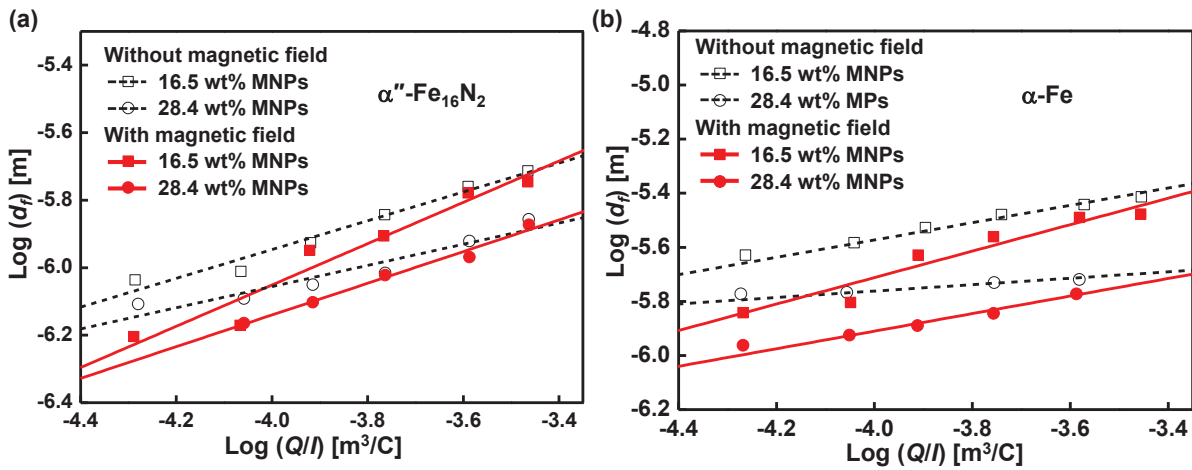


Figure 4.6. Plots of $\log d_f$ (average nanocomposite fiber diameter) against $\log(Q/I)$ at different MNP loadings. (a) and (b) are the α'' -Fe₁₆N₂/PVP and α -Fe/PVP nanocomposite fibers, respectively.

The difference in the exponent from that in the model developed by Fridrikh et al may be due to the solution properties (viscosity and conductivity) and the MNPs embedded in the fibers. The model developed by Fridrikh et al neglects the effect of viscosity and conductivity on the final fiber diameter. Viscosity may play a role in determining the rate of jet thinning in the system between the nozzle and asymptotic [21]. By embedding MNPs, the conductivity of the precursor increased, which increased the current flow through the fibers. This would lead to a decrease in the diameter of the fiber.

The power coefficients of α -Fe fibers were lower than that of α'' -Fe₁₆N₂ fibers. However, the power coefficients of both fibers are still lower than that obtained from model, which is 0.667. Increasing the magnetic NP loading also increased the power coefficient for fibers prepared both without and with a magnetic field. However, application of the magnetic field decreased the power coefficient, with a greater decrease experienced by α -Fe fibers. These show the effect of the magnetic properties of the NPs embedded on fiber formation, namely that α'' -Fe₁₆N₂ NPs have a stronger effect than α -Fe NPs. The magnetic strength increases with increasing numbers of NPs in the fibers. This result also shows that the effect of magnetic field is more significant on α'' -Fe₁₆N₂ fibers than that of α -Fe fibers. For the α'' -Fe₁₆N₂ fibers, the effect of the magnetic NPs was greater than that of the applied magnetic field. This verifies that the fiber diameter decreases on application of a magnetic field. The difference in the intercept value was dependent on the ferrofluid properties.

Table 4.4. Power law exponents of prepared fibers under various conditions

Fibers	MNPs loading	16.5 wt%			28.4 wt%		
		Slope	Intercept	R ² value	Slope	Intercept	R ² value
α'' -Fe ₁₆ N ₂	Without magnetic field	0.469	-4.263	0.979	0.612	-3.604	0.929
	With magnetic field	0.314	-4.802	0.895	0.427	-4.239	0.960
α -Fe	Without magnetic field	0.325	-4.612	0.966	0.489	-3.756	0.946
	With magnetic field	0.119	-5.287	0.847	0.320	-4.291	0.964

4.3.4.2. Effect of applied magnetic field on fibers diameter

The large improvement in fiber uniformity can be attributed to the control of the cone-jet geometry by an electric current or reduction of the spinning jet instability by applying a magnetic field during electrospinning [22, 23]. The magnetic field can balance the force that reduces the instability that can cause formation of branched fibers. Under a magnetic field, the current generates a centripetal ampere force, F_m , on the jet, the direction of which is towards the initial equilibrium point [24].

$$F_m = \frac{1}{c} \left[q_e u \times B + I \times B + c(\nabla B) \cdot M + (P \times B) \cdot u + \frac{\partial}{\partial t} (P \times B) \right] \quad (4.2)$$

where q_e is the electric charge, B is the magnetic induction, I is the current, M is the magnetization, P is the polarization, u is the velocity of the jet, and c is the velocity of light in a vacuum. The produced F_m will lead to a straightened whipping circle, resulting in an increase in the velocity of the moving jet (u). In other words, an increase in F_m results the increase in u , ($u \propto F_m$). According to mass conservation, the diameter of the fiber decreases with increasing velocity of the jets ($d_f^2/4 \sim 1/u$). This means that the fiber diameter decreases on application of a magnetic field. Furthermore, the decrease in the diameter of the whipping circle increases the cone-jet stability, which will drive production of a more uniform fiber.

4.3.5. Magnetic properties of electrospun magnetic nanocomposite fibers

The magnetic properties of the α'' -Fe₁₆N₂ nanocomposite fibers prepared without and with a magnetic field were evaluated from the hysteresis curves. **Figure 4.7** shows the magnetic properties of the nanocomposite fibers, obtained by SQUID analysis at 300 K, where an extremely high magnetization was observed. The measured saturation magnetization (M_s) values of the magnetic fibers prepared by electrospinning were 44.01 and 49.29 emu g⁻¹ for

fibers prepared without and with a magnetic field, respectively. The M_s value of the fibers prepared with a magnetic field was slightly higher than that of the fibers prepared without an applied magnetic field, which may be due to the different number of magnetic NPs inside the fibers. The M_s values of the prepared fibers were smaller than that of the α'' -Fe₁₆N₂ NPs (144 emu g⁻¹) due to the effect of the polymer mass in the nanocomposite fibers.

The magnetic coercivity of the fibers prepared without the magnetic field was 0.83 kOe. After applying magnetic field, H_c was enhanced to 1.02 kOe. This result indicates that the magnetic moments of the NPs were aligned by the magnetic field, which means that alignment of the particles in the fibers significantly enhanced the magnetocrystalline anisotropy of the fibers, increasing their magnetic performance. The H_c value of the nanocomposite fibers is smaller than that of the α'' -Fe₁₆N₂ NPs (2.3 kOe). The magnetic remanence values of the fibers prepared without and with a magnetic field were 7.37 and 9.01 emu/g. The hysteresis curve of the α'' -Fe₁₆N₂ magnetic NPs shows a great increase on magnetization by applying a small magnetic field. This implies that α'' -Fe₁₆N₂ NPs have a sensitive magnetic property, which is a promising feature for application in magnetic sensors.

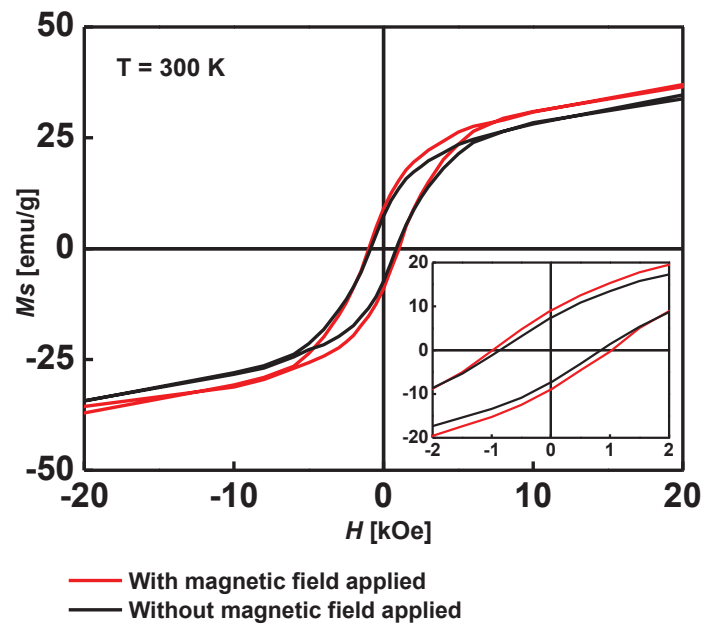


Figure 4.7. Hysteresis curves of nanocomposite α'' -Fe₁₆N₂/PVP magnetic fibers with an MNP loading of 28.4 wt%.

The core-shell α'' -Fe₁₆N₂ NPs were spherical particles dispersed as single-domain NPs. Their surfaces were covered with surfactant molecules, enabling the magnetic NPs to rotate freely in their positions. Fixing the magnetic NPs inside the fibers would prevent degradation of the NP performance and agglomeration caused by the coupling magnetic moment. **Figure**

4.8 (a) shows the initial SQUID analysis of the α'' -Fe₁₆N₂ fibers. The curve slope of the fibers prepared with a magnetic field indicates that the applied magnetic field caused the magnetic NPs to align inside the fibers. The possible magnetic NP directions inside the fibers based on these results are shown in **Figure 4.8** (b). The applied magnetic field promoted the alignment of the magnetic NPs, which led to a reduction in the fiber diameter. Without the magnetic field, the magnetic NPs were randomly distributed inside the fiber. After applying a magnetic field, the NPs aligned along the fiber and formed a chain. During electrospinning, the magnetic moment of the NPs was perfectly aligned along the fiber length due to the external magnetic field. After deposition on the collector, the direction of the magnetic moments was slightly changed along the magnetic field direction as the particle moved closer to the external applied magnet.

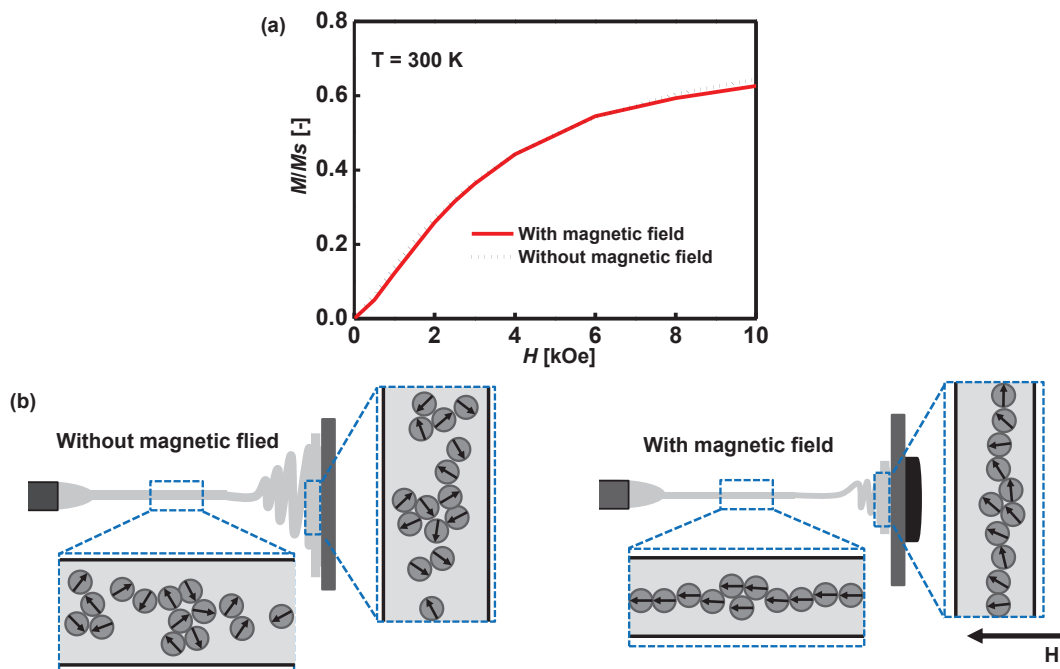


Figure 4.8. (a) Initial SQUID analysis of nanocomposite α'' -Fe₁₆N₂/PVP magnetic fibers with a MNP loading of 28.4 wt%. (b) Schematic diagram of possible magnetic particle directions inside fibers prepared without and with a magnetic field.

4. 4 Conclusion

The morphology of two kinds of magnetic nanocomposite fiber with either core-shell single-domain α'' -Fe₁₆N₂/Al₂O₃ or α -Fe/Al₂O₃ NPs embedded in PVP as a function of flow rate was examined in a magneto-electrospinning system. In this system, an external magnetic field of 0.1 T was applied parallel to the electric field. The experimental results showed that the

applied magnetic field gave the fiber a smaller diameter and a more uniform distribution. The higher loading of either α'' -Fe₁₆N₂ or α -Fe NPs in the fiber resulted in smaller diameters than the lower loading. It was found from the TEM observation that the α'' -Fe₁₆N₂ NPs were aligned stably in one dimension along the longer direction of the fiber. No change in the crystal structure of α'' -Fe₁₆N₂ due to the electrospinning was observed. Further, the SQUID measurements for the 28.4 wt% loading of α'' -Fe₁₆N₂ NPs revealed an extremely high saturation magnetization of 49 emu/g with a coercivity of 1 kOe. These results suggest the potential of constructing bulk magnetic materials using α'' -Fe₁₆N₂ NPs, which furthermore reveals promising features for many other magnetic applications, such as magnetic sensors.

4. 5 References

- [1] Eid C, Brioude A, Salles V, Plenet JC, Asmar R, Monteil Y, Khoury R, Khoury A, Miele P 2010 Iron-based 1D nanostructures by electrospinning process *Nanotechnology* **21** 125701
- [2] Wu H, Zhang R, Liu X, Lin D, Pan W 2007 Electrospinning of Fe, Co, and Ni nanofibers synthesis, assembly, and magnetic properties *Chem. Mater.* **19** 3506–11
- [3] Park KY, Han JH, Lee SB, Kim JB, Yi JW, Lee SK 2009 Fabrication and electromagnetic characteristics of microwave absorbers containing carbon nanofibers and NiFe particles *Compos. Sci. Technol.* **69** 1271-8
- [4] Ghasemi E, Ziyadi H, Afshar AM, Sillanpää M 2015 Iron oxide nanofibers: A new magnetic catalyst for azo dyes degradation in aqueous solution *Chem. Eng. J.* **264** 146-51
- [5] Fei L, Hu Y, Li X, Song R, Sun L, Huang H, Gu H, Chan HL, Wang Y 2015 Electrospun bismuth ferrite nanofibers for potential applications in ferroelectric photovoltaic devices *ACS Appl. Mater. Interfaces* **7** 3665-70
- [6] Kim YJ, Ebara M, Aoyagi T 2013 A smart hyperthermia nanofiber with switchable drug release for inducing cancer apoptosis *Adv. Funct. Mater.* **23** 5753-61
- [7] Munir MM, Iskandar F, Khairurrijal, Okuyama K 2009 High performance electrospinning system for fabricating highly uniform polymer nanofibers *Rev. Sci. Instrum.* **80** 026106
- [8] Yang D, Lu B, Zhao Y, Jiang X 2007 Fabrication of aligned fibrous arrays by magnetic electrospinning *Adv. Mater.* **19** 3702-6

- [9] Wang H, Tang H, He J, Wang Q 2009 Fabrication of aligned ferrite nanofibers by magnetic-field-assisted electrospinning coupled with oxygen plasma treatment *Mater. Res. Bull.* **44** 1676-80
- [10] Ajao JA, Abiona AA, Chigome S, Fasasi AY, Osinkolu GA, Maaza M 2010 Electric-magnetic field-induced aligned electrospun poly (ethylene oxide) (PEO) nanofibers *J. Mater. Sci.* **45** 2324-9
- [11] Ogawa T, Ogata Y, Gallage R, Kobayashi N, Hayashi N, Kusano Y, Yamamoto S, Kohara K, Doi M, Takano M, Takahashi M 2013 Challenge to the synthesis of α "-Fe₁₆N₂ compound nanoparticle with high saturation magnetization for rare earth free new permanent magnetic material *Appl. Phys. Express* **6** 073007
- [12] Ogi T, Nandiyanto ABD, Kusakibaru Y, Iwaki T, Nakamura K, Okuyama K 2013 Facile synthesis of single-phase spherical α "-Fe₁₆N₂/Al₂O₃ core-shell nanoparticles via a gas-phase method *J. Appl. Phys.* **113** 164301
- [13] Zulhijah R, Yoshimi K, Nandiyanto ABD, Ogi T, Iwaki T, Nakamura K, Okuyama K 2014 α "-Fe₁₆N₂ phase formation of plasma-synthesized core-shell type α -Fe nanoparticles under various conditions *Adv. Powder Technol.* **25** 582-90
- [14] Zulhijah R, Nandiyanto ABD, Ogi T, Iwaki T, Nakamura K, Okuyama K 2015 Effect of oxidation on α "-Fe₁₆N₂ phase formation from plasma-synthesized spherical core-shell α -FeAl₂O₃ nanoparticles *J. Magn. Magn. Mater.* **381** 89-98
- [15] Zulhijah R, Suhendi A, Yoshimi K, Kartikowati CW, Ogi T, Iwaki T, Okuyama K 2015 Low-energy bead-mill dispersion of agglomerated core-shell α -Fe/Al₂O₃ and α "-Fe₁₆N₂/Al₂O₃ ferromagnetic nanoparticles in toluene *Langmuir* **31** 6011-9
- [16] Guo Z, Lin H, Karki AB, Wei S, Young DP, Park S, Willis J, Hahn TH 2008 Facile monomer stabilization approach to fabricate iron-vinyl ester resin nanocomposites *Compos. Sci. Technol.* **68** 2551-6
- [17] Li P, Liu C, Song Y, Niu X, Liu H, Fan Y 2013 Influence of Fe₃O₄ nanoparticles on the preparation of aligned PLGA electrospun fibers induced by magnetic field *J. Nanomater.* **2013** 1-9
- [18] Liu Y, Zhang X, Xia Y, Yang H 2010 Magnetic-field-assisted electrospinning of aligned straight and wavy polymeric nanofibers *Adv. Mater.* **22** 2454-7
- [19] Fernández De La Mora J, Loscertales IG 1994 The current emitted by highly conducting Taylor cones *J. Fluid Mech.* **260** 155-84

- [20] Fridrikh SV, Yu JH, Brenner MP, Rutledge GC 2003 Controlling the fiber diameter during electrospinning *Phys. Rev. Lett.* **90** 144502
- [21] Rutledge GC, Fridrikh SV 2007 Formation of fibers by electrospinning *Adv. Drug Deliver. Rev.* **59** 1384-91
- [22] Suhendi A, Munir MM, Suryamas AB, Nandiyanto ABD, Ogi T, Okuyama K 2013 Control of cone-jet geometry during electrospray by an electric current *Adv. Powder Technol.* **24** 532-6
- [23] Wu Y, Yu JY, He JH, Wan YQ 2007 Controlling stability of the electrospun fiber by magnetic field *Chaos Solitons Fractals* **32** 5-7
- [24] Xu L 2009 A mathematical model for electrospinning process under coupled field forces *Chaos Solitons Fractals* **42** 1463-5

Chapter 5

Summary and conclusion

Magnetic materials play a key role in modern life since these magnetic materials have been currently being applied in human life and industrial applications, such as magnetic recording devices, motor, biomedical, sensor, spintronic devices, energy alternatives, etc. α'' -Fe₁₆N₂ nanoparticles (NPs), which have the highest magnetic moment among the ferromagnetic materials, has believed as a potential new rare-earth-free magnetic material. However, α'' -Fe₁₆N₂ NPs has strong magnetic interaction among NPs which lead to small magnetic coercivity value. Therefore, a method to enhance the magnetic performance of this NPs is highly desired for new generation of high performance magnetic materials. Alignment of the magnetic moment of the α'' -Fe₁₆N₂ NPs resulted in an enhancement of their magnetic properties. Therefore, detailed understanding on the preparation of magnetically aligned α'' -Fe₁₆N₂ nanocomposite and their magnetic performance are highly desired to make clear the application of this material for the formation of high performance of rare-earth-free magnetic material.

In this dissertation, the synthesis of α'' -Fe₁₆N₂ magnetic NPs composites were successfully prepared from well-dispersed single phase core-shell α'' -Fe₁₆N₂/Al₂O₃ NPs which are synthesized from α -Fe/Al₂O₃ by reduction and nitridation process followed by dispersion of the nitrated samples using bead-mill dispersion process. The α'' -Fe₁₆N₂ NPs composites were prepared by spin-coating for film and electrospinning for fibers under applied external magnetic field. For the conclusion of the dissertation, the major results are summaries as follows:

1. Nanostructured spherical core-shell single-domain α'' -Fe₁₆N₂/Al₂O₃ NPs films were prepared by spin-coating of well-dispersed core-shell α'' -Fe₁₆N₂/Al₂O₃ NPs in toluene. The spherical α'' -Fe₁₆N₂ NPs were aligned under an applied magnetic field of 1.2 T during spin coating. XRD results confirmed the successful alignment of the core-shell α'' -Fe₁₆N₂/Al₂O₃ NPs in the film. Kerr effect evaluation showed that the spin-coated core-shell α'' -Fe₁₆N₂/Al₂O₃ NPs had a higher H_c of 3.5 kOe than the as-prepared α'' -Fe₁₆N₂/Al₂O₃ NPs (2.5 kOe). SQUID analysis shows the increase in H_c and M_r of 22.7% and 55.2%, respectively, after the application of magnetic field.
2. The effect of magnetic field strength on the alignment of single-domain α'' -Fe₁₆N₂/Al₂O₃ NPs films were investigated in detail. The XRD and SQUID analyses

show increases in the alignment of the magnetic moment of the NPs and the magnetic properties with the increase in the magnetic field applied vertically to the film substrate. At 1.2 T, the alignment of the magnetic moment increased by 35%, whereas the H_c , M_r , and $(BH)_{\max}$ increased by 24%, 66%, and 160%, respectively. The maximum H_c and $(BH)_{\max}$ values can be estimated from the relationship between the alignment of the magnetic orientation and the magnetic properties to be approximately 8 kOe and 7 MGOe, respectively.

3. The morphology of magnetic nanocomposite fiber with core-shell single-domain α'' - $Fe_{16}N_2/Al_2O_3$ NPs embedded in PVP as a function of flow rate was examined in a magneto-electrospinning system. In this system, an external magnetic field of 0.1 T was applied parallel to the electric field. The experimental results showed that the applied magnetic field gave the fiber a smaller diameter and a more uniform distribution. The higher loading of α'' - $Fe_{16}N_2$ NPs in the fiber resulted in smaller diameters than the lower loading. It was found from the TEM observation that the α'' - $Fe_{16}N_2$ NPs were aligned stably in one dimension along the longer direction of the fiber. No change in the crystal structure of α'' - $Fe_{16}N_2$ due to the electrospinning was observed. Further, magnetic hysteresis curves showed an enhancement of the magnetic coercivity (H_c) and remanence (M_r) by 22.9% and 22.25%, respectively.

From the conclusions stated above, it can be highlighted that the magnetic performance of the α'' - $Fe_{16}N_2/Al_2O_3$ NPs can be enhanced by aligning the magnetic moment of the NPs. The highest magnetic performance of α'' - $Fe_{16}N_2$ materials can be achieved by perfectly aligning their magnetic moment under higher applied magnetic field. These results imply that core-shell single-domain α'' - $Fe_{16}N_2/Al_2O_3$ NPs have the potential for the construction of bulk magnetic materials with tunable magnetic performances by applying a magnetic field. The results of this research also showed that the magnetic properties of magnetic materials can be tuned by tuning their magnetic moment. This magnetic property tuning process is also possible to be applied to other magnetic materials.

Acknowledgment

First of all, I would like to express my gratitude to my supervisor, Associate Professor Takashi Ogi for providing very helpful advice, guidance, continuing encouragement not only research but also daily life.

I also would like to thank Professor Akihiro Yabuki, Professor Shigeki Takishima, and Professor Kei Inumaru for their patience, wisdom and support as referee members. And special thanks to Professor Kikuo Okuyama, Dr. Toru Iwaki, Assistant Professor Ratna Balgis, and Dr Takahiro Onimaru for their great advices and supports during my research. I am grateful to Dr, Asep Suhendi and Dr. Rizka Zuhijah for willingness supports my research during their stay in Hiroshima University. I also want to thank for the past and present friends in Okuyama laboratory, Dr. Osi Arutanti, Aditya Farhan Arif, Ghana Rinaldi, Fitri Aulia permatasari, Lusi Ernawati, and other Japanese members for their kind helps and assistances during my research and daily life.

I thank funding from Ministry of Education, Culture, Sports, Science and Technology for providing scholarship of my PhD course and Hosokawa Micron Powder Foundation for financial support of my research.

Last but not least, I would like to really thank my late father, Sudarta, my mother, Hartatik, my sister, Chandra Kirana Wahyu Ningrum, and my brothers, Nurul Priyanto and Anton Wahyudi, for their prayers, support, and motivation. It is beyond words. Without these, I might not be able to achieve anything.

CHRISTINA WAHYU KARTIKOWATI

Higashi Hiroshima, September 2017

List of Publications

1. R. Balgis, Christina W. Kartikowati, T. Ogi, L. Gradon, L. Bao, K. Seki, K. Okuyama: Synthesis and evaluation of straight and bead-free nanofibers for improved aerosol filtration, **Chemical Engineering Science** 2015, 137, 947-954.
2. R. Zulhijah, A. Suhendi, K. Yoshimi, Christina W. Kartikowati, T. Ogi, T. Iwaki, K. Okuyama: Low-energy bead-mill dispersion of agglomerated core-shell α -Fe/Al₂O₃ and α'' -Fe₁₆N₂/Al₂O₃ ferromagnetic nanoparticles in toluene, **Langmuir**. 2015, 31, 6011-6019.
3. A. Suhendi, Christina W. Kartikowati, R. Zulhijah, T. Ogi, T. Iwaki, K. Okuyama: Preparation and characterization of magnetic films of well dispersed single domain of core-shell α'' -Fe₁₆N₂/Al₂O₃, **Advanced Powder Technology**. 2015, 26, 1618-1623.
4. Christina W. Kartikowati, A. Suhendi, R. Zulhijah, T. Ogi, T. Iwaki, K. Okuyama: Preparation and evaluation of magnetic nanocomposite fibers containing α'' -Fe₁₆N₂ and α -Fe nanoparticles in polyvinylpyrrolidone via magnetoelectrospinning, **Nanoscale** 2016, 8, 2648-2655.
5. Christina W. Kartikowati, A. Suhendi, R. Zulhijah, T. Ogi, T. Iwaki, K. Okuyama: Effect of magnetic field strength on the alignment of α'' -Fe₁₆N₂ nanoparticle films, **Nanotechnology**. 2016, 27, 025601.
6. Q. Li, Christina W. Kartikowati, T. Ogi, T. Iwaki, K. Okuyama: Facile fabrication of carbon nanotube forest-like films via coaxial electrospay, **Carbon** 2017, 115 116–119.